IEEE Access
Multidisciplinary ⋮ Rapid Review ⋮ Open Access Journal

Received 11 August 2023, accepted 16 October 2023, date of publication 23 October 2023, date of current version 31 October 2023.

Digital Object Identifier 10.1109/ACCESS.2023.3326950

RESEARCH ARTICLE

Distribution Network Power Quality Insights With Optimally Placed Micro-PMUs Incorporating Synthetic and Real Field Data

MANOJ PRABHAKAR ANGUSWAMY, (Member, IEEE), MANOJ DATTA, (Senior Member, IEEE), LASANTHA MEEGAHAPOLA, (Senior Member, IEEE), AND ARASH VAHIDNIA, (Senior Member, IEEE)

School of Engineering, Royal Melbourne Institute of Technology (RMIT) University, Melbourne, VIC 3000, Australia

Corresponding author: Manoj Prabhakar Anguswamy (manoj.anguswamy@student.rmit.edu.au)

This work was supported by the Royal Melbourne Institute of Technology (RMIT) University RTP Stipend Scholarship (RSS).

ABSTRACT Widespread deployments of optimally placed real-time power quality (PQ) monitoring tools such as distribution level micro-phasor measurement units (D-PMUs or μPMU), digital fault recorders, and PQ analyzers are expected to play a critical role in improving the stability and reliability of the smart grid. In this paper, an improved PQ disturbance (PQD) classification method using discrete wavelet transform (DWT) with a cubic multi-class support vector machine (CMSVM) classifier is proposed, which incorporates a decade's worth of high-quality continuous waveform PQ data from the Australian power network. This research also introduces misclassification cost (MC) and cost-sensitive classification theory into the area of PQD classifiers to build improved and more robust network models for the future. The method is evaluated using four case studies of synthetic and real-world PQD field data combinations and five application case studies using optimally placed μPMUs. The results indicate similar classification performance for standard PQDs than previous literature, alongside improved MC for complex PQD classes. Comparative analysis with previous literature highlights the importance of using high-quality real PQD field data to improve the fidelity of classifiers to provide better PQ insights as more complex components are added to the distribution network.

INDEX TERMS Distribution network, micro-PMU, optimal placement, power quality insights.

NOMENCLATURE

μPMU:	Micro phasor measurement unit.
ADALINE:	Adaptive linear network.
ADN:	Active distribution network.
CMSVM:	Cubic multi-class support vector machine.
CNN:	Convolutional neural network.
CWT:	Continuous wavelet transform.
DFR:	Digital fault recorder.
DL:	Deep learning.
DPMU:	Distribution phasor measurement unit.
DSO:	Distribution system operator.
DT:	Decision tree.
DWT:	Discrete wavelet transform.
EEMD:	Ensemble empirical mode decomposition.
FFNN:	Feedforward neural network.
KNN:	K-nearest neighbor.
LSTM:	Long short-term memory.
MC:	Misclassification cost.
ML:	Machine learning.
MRA:	Multi-resolution analysis.
MSVM:	Multi-class support vector machine.
OCA:	Overall classification accuracy.
PNN:	Probabilistic neural network.
PQ:	Power quality.
PQA:	Power quality analyzer.

The associate editor coordinating the review of this manuscript and approving it for publication was Ali Raza.

PQD:	Power quality disturbance.
RF:	Random forest.
RNN:	Recurrent neural network.
SNR:	Signal-to-noise ratio.
ST:	Stockwell transform.
UDNA:	Unique distribution network attributes.
UNP:	Unknown network parameters.
UZIP String	Usable zero-injection phase strings.
VMD:	Variable mode decomposition.
XAI:	Explainable artificial intelligence.

I. INTRODUCTION

The increasing number of complex power electronic components with widespread renewable adoption has made the active distribution network (ADN) prone to instability, causing power quality (PQ) issues. Previously unseen demand dynamics have made it difficult for distribution system operators (DSOs) to provide reliable electrical supply with the appropriate voltage, frequency, and waveform shape while staying within acceptable standard limits [1]. In this context, there is a significant push to enhance real-time situational awareness with better PQ in all system conditions. To improve PQ, it is necessary to proactively identify the sources and causes of PQ disturbances (PQDs). This requires detecting, localizing, and classifying the type of PQD so appropriate mitigating action can be taken.

Recent literature [2], [3] has highlighted the importance of using a high sampling rate of modern measurement tools in classifying PQDs. Hence, increased grid visibility can be realized by incorporating heterogeneous data from PQ analyzers (PQA), digital fault recorders (DFRs), and distribution-level micro phasor measurement units (D-PMUs, micro-PMUs or μPMUs) into a new consolidated framework [4] for better PQD identification and fault analysis. However, previous literature [2], [3], [5], [6], [7], [8], [9], [10], [11], [12], [13], [14], [15], [16], [17], [18], [19], [20], [21], [22], [23], [24], [25], [26], [27], [28], [29], [30], [31], [32] and their proposed methods which performed proficiently with synthetic data, have not incorporated high-quality, real-field data into their PQD classification methodology. They have been limited to data from less accurate legacy measurement devices such as transmission level PMUs, a small subset of field data, or experimental setups.

There are two sequential steps in developing a PQD classification technique: feature extraction and classification. Optimal feature extraction for PQD classifiers plays a pivotal role in a specific method's overall efficiency, accuracy, and real-time applicability. In [33], an automatic feature selection algorithm was developed, with the most useful parameters defined for the classifier to optimize speed and accuracy. However, the features extracted using other techniques such as variable mode decomposition (VMD) [22], ensemble empirical mode decomposition (EEMD) [32], and adaptive linear network (ADALINE) [14] were stated to be computationally intensive and unsuitable for real-time implementation.

The authors in [29] evaluated various classifiers such as k-nearest neighbor (KNN), random forest (RF), and support vector machines (SVM). The authors noted that feature selection plays a crucial role in the performance and sensitivity of the classifier; however, real-world performance cannot be evaluated with synthetic data alone. Whereas, in [34], the SVM classifier achieved higher real-PQD accuracy when trained on a combination of real power networks and synthetic data.

The discrete wavelet transform (DWT) feature extraction technique used in [17] indicated a good equilibrium of accuracy with improved computational efficiency compared to previous Stockwell transform (ST) methods. In [8] and [19], the author used DWT to extract energy and entropy characteristics at various resolutions to classify PQDs using a probabilistic neural network (PNN) with suitable real-time applicability.

In [19], an eight-level DWT optimal feature selection algorithm was developed. However, there are marginal gains in performance compared to a more efficient four-level [29] or six-level [27] wavelet decomposition method. In both studies, important PQ indies, such as total harmonic distortion (THD) and flicker measurements, and their effect on classifier performance were not explored.

Various kernel SVM types were evaluated in [9], [11], [18], [32], and [34]. However, there is limited research on the performance of the cubic multi-class SVM (MSVM) kernel with standard and complex PQDs.

There have been many other combinations of approaches developed to detect and localize PQDs, including ST and PNN approaches [7], [12], ST and decision trees (DT) [3], [10], and DWT multi-resolution analysis (MRA) with decision-making architecture [5]. Researchers have also explored threshold-based approaches using a feedforward neural network (FFNN) classifier with synthetic synchrophasor data [20], showing good overall classification accuracy (OCA) of standard PQDs. However, it is difficult to obtain real field data of μPMUs, since it is a new technology that has been recently embraced.

With more convoluted elements added to ADNs, it is expected that more advanced or complex PQDs combining double, triple, or quadruple PQDs will occur more frequently. In [27], OCA deteriorated as the number of PQD classes increased, especially with complex PQDs. Therefore, a PQD classifier method must be developed to accommodate such scenarios. Previous literature [2], [3], [4], [5], [6], [7], [8], [9], [10], [11], [12], [13], [14], [16], [17], [18], [19], [20], [21], [22], [23], [24], [25], [26], [29], [31], [33], [34], [35] has only evaluated their proposed method with basic or standard PQDs listed in the IEEE standards or a few complex PQDs. Research into more complex PQD classifier performance has been largely unexplored.

Recently, deep learning (DL) models [21], [24], [26], [36], [37], [38], [39], [40], [41], [42], [43], [44] have gained a

TABLE 1. Comparison of Different Classifiers for PQD Classification in Literature.

Method	Ref	Advantages	Disadvantages
SVM	[9, 11, 17, 18, 23, 32-34]	High learning ability; proficient performance with unseen PQD data; ability to map non-linear decision boundaries; versatile, tunable, and customizable kernel functions	Increased training time for a large PQD dataset; requires strict preprocessing of PQD training dataset through normalization and segmentation; performance heavily dependent on PQD data quality
PNN	[7, 8, 12, 19]	Informed multi-class classification with an estimation of probabilities; fast training and prediction times; minimal preprocessing required	Very sensitive to the choice of initial parameters which affects performance; sensitive to initially chosen weights and prone to convergence; requires large PQD training data
FFNN	[7, 14]	Ability to handle large and complex PQD datasets with good generalization ability	Difficult to train; very sensitive to hyperparameter configuration and optimization
DT	[3, 10, 22]	Fast training and prediction speeds; low computational burden	Prone to overfitting with many complex PQD classes; possibility to have biased predictions towards certain class of PQDs
DL	[21, 24, 26, 36-44]	High self-learning ability for complex PQD patterns and features; customizable scalable architecture.	Substantial amount of high quality labeled PQD field data required; computationally intensive; optimal performance requires careful hyperparameter tuning

lot of traction, which include techniques such as recurrent neural networks (RNN), long short-term memory (LSTM), and convolutional neural networks (CNN), among others. However, they utilize no real-field data [36], [37], [39], [40], [41], [42], [44] or extremely limited legacy datasets [21], [26], [38], [43] with low instrument sampling rates [37], [40], [41], [42], [43], [44].

As shown in [38], where limited real-field data is used, if misclassification occurs, then the subsequent decisions will be critically affected. Consequently, the manual labeling of tens of thousands of real-field PQDs is required [36], [38], [43] to develop a robust DL method in the future. Moreover, when synthetically trained DL models were tested on a small subset of real-field data, there was a significant drop in OCA of 6% [21] and 9% [26]. Accordingly, the limitations of DL techniques are the increased complexity of network models, poor generalization, overfitting, and lack of high-quality field PQDs to make them suitable for deployment.

It is also difficult to understand why a particular machine learning (ML) algorithm performs better than others with a simple OCA metric. The authors in [34] evaluated different combinations of synthetic and real-field datasets and their effect on the MSVM classifier. Similarly, researchers in [31] developed a CNN with explainable artificial intelligence (XAI) for evaluating and measuring the trustworthiness of ML techniques for PQDs classifiers. Despite this, all previous studies have neglected the importance of cost-sensitive classification in the problem formulation of PQD classification. The evaluation of different classifier methods is shown in Table 1.

The idea of misclassification costs (MC) is frequently seen in the medical field [45] and relates to the potential consequences of incorrectly classifying a high-risk class as a low-risk class. MC is critical for specialized PQ engineers and DSOs who will rely upon the precise classification of PQDs to improve their productivity. This aspect is missing from all previous publications.

While some PQD classification methods have incorporated smart meter data [16], [46], these non-standardized devices cannot capture dynamic responses affecting PQD classification and distribution system state estimation (DSSE). Measurement tools such as DFRs and PQAs with integrated μPMU functionality [47] have been recently developed, making it possible for real-time and historical PQ emissions capture and assessment through newly developed linear DSSE [48] and PQ software. These devices are smaller, more accurate, and less expensive than conventional transmission level PMUs [49], with reporting rates between 10-240 frames per second, improved total vector error (TVE) [47], and better dynamic performance as per the updated IEC/IEEE 60255-118-1 standard [50].

Class P μPMUs are used for protection applications, whereas Class M μPMUs are suitable for PQ applications due to their greater embedded filtering. The resultant GPS time-stamped measurements from μPMUs placed throughout ADNs enables precise tracking of magnitude and phase fluctuations at the node and nearby feeders.

However, the valuable PQ insights of deploying these devices for DSOs heavily depend on their optimal placement. Our paper [51] presented a new state-of-the-art μPMU ADN optimal placement method which considers the unique distribution network attributes (UDNA) in the usable zero-injection phase string (UZIP String) placement algorithm.

This paper makes the following significant contributions to address the shortcomings of previous literature.

- An improved traditional ML method using DWT and cubic-kernel MSVM (CMSVM) that combines previous literature's best attributes is developed and evaluated for both standard and complex PQDs.
- For the first time, the notion of MC is introduced in PQD classification methodology, and how it is beneficial and valuable to build robust DL methods in the future. A hand-crafted feature set to reduce MC is established

alongside new features like flicker measurements. This is unseen in previous literature.
- The uniqueness of this study is that it uses decades' worth of high-quality, real-world field PQD data from the Australian Distribution Network and is not limited to legacy PQ databases and instruments.
- The assessment and implications of ML behavior when the classifier is trained on combinations of synthetic and a large stream of real-field data is evaluated.
- Computational efficiency is improved by utilizing the most effective pre-processing techniques, such as segmentation, normalization, and noise filtering with the same DWT MRA decomposition as the feature extraction.
- The importance of optimal μPMU placement infrastructure in ADNs to provide valuable PQ insights is explored through five in-depth PQ application case studies considering the state-of-the-art UZIP String μPMU placement method. This application aspect is missing from previous literature.
- Other contributions include evaluating different wavelet types, decomposition levels, and their effect on OCA. The impacts of various instrument sampling rates on the proposed method. Additional laboratory tests with μPMUs, DFRs, and PQAs, their latency, and computational burden with the proposed method are also assessed.

This paper is organized as follows. Section II introduces MRA elements of DWT and concepts for the cost-weighted CMSVM classifier. Section III details the synthetically generated dataset and real PQD field data. Section IV presents the proposed methodology. In Section V, performance evaluation for four case studies is presented. Section VI, the importance of optimally placed μPMUs in ADNs is assessed with five application case studies. Lastly, Section VII compares the proposed method with previous literature, limitations, practical constraints, and added benefits with some future research directions.

II. IMPROVED DWT MRA WITH MC WEIGHTED CLASSIFIER

A. DISCRETE VS CONTINUOUS WAVELET TRANSFORM

The DWT is a mathematical technique that decomposes a signal into a set of wavelets, which are functions that are localized in both time and frequency. The difference between DWT and continuous wavelet transform (CWT) is based on the translation and scaling parameters. In CWT, both parameters can be tuned finely, whereas DWT is fixed and has discretized scaling factor of two. DWT is preferred for real-time computational environments [33] such as detection of PQDs and will be used in this research.

B. CHOICE OF MOTHER WAVELET AND DECOMPOSITION LEVEL

The choice of the mother wavelet and coefficient choice impacts the detection and localization of PQDs due to time delay and overdamping of transients [2]. Many studies [5], [8], [9] imply four-coefficient Daubechies' wavelet (Daub4 or Db4) performs better than other wavelets with a small computational cost due to the short wavelet filter. However, there has not been conclusive comparative analysis to validate these claims.

Consequently, in preliminary tests, different wavelet families and their best members were tested alongside different levels of decomposition with an equal combination of synthetic and real field data. It was found that the best performing wavelets were the Biorthogonal 3.7 and Db4 wavelets. As shown in Fig. 1, the Bior3.7 and Db4 wavelets had identical OCA performance at four, six, and eight level decomposition levels. In all wavelet types, going from three to four-level decomposition had the biggest improvement in OCA. In this study, the Db4 mother wavelet is chosen with eight-levels of decomposition for the best OCA.

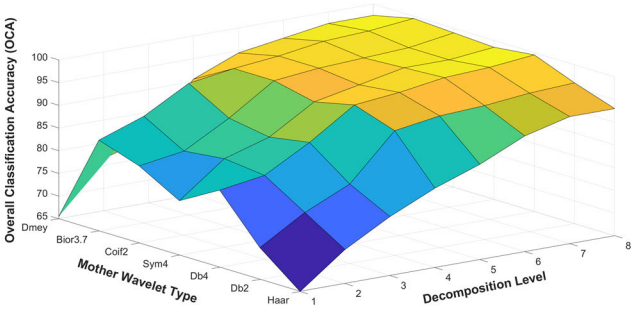

FIGURE 1. Relationship between different mother wavelet types, decomposition levels, and overall classification accuracy of PQDs.

C. IMPLEMENTATION OF NOISE FILTER

The major drawback of DWT is its ability to reject noise given different types of mother wavelets. Different wavelet types were tested in noisy environments [9], showing that the best-performing Db4 wavelet can still achieve great classification accuracy. In this study, a noise filter that uses the same Db4 wavelet and eight-level decomposition is utilized for the denoising algorithm to improve the efficiency of the proposed method. Impulse noise, which closely resembles electrical noise, is used alongside a universal hard-thresholding method for denoising. This DWT noise filter can be turned on or off depending on the noise level or signal-to-noise ratio (SNR) of the incoming signal or considering the type of filtering used in the instrument itself. For example, Class M μPMU has greater filtering than Class P μPMUs. In this research, the noise filter was turned off for the real-field data. Practical noise considerations for PQ monitoring are later discussed.

D. CUBIC MULTI-CLASS SUPPORT VECTOR MACHINE (CMSVM)

This research uses the cubic kernel MSVM and DWT for MRA to classify standard and complex PQDs. Previous studies [9], [11], [18], [32], [34] have used popular kernels such as linear, radial basis function (RBF), or sigmoid kernels.

Different kernel types were evaluated, and it was found that the cubic SVM kernel produced consistently better results than other types in the proposed method. This was especially evident as the number of complex PQDs increased. The CMSVM kernel utilizes a degree-3 polynomial, excels in modeling non-linear or unbalanced decision boundaries such as PQD classification and can capture more intricate details than a lower-degree polynomial kernel.

For instance, the decision boundary overlaps with more complex triple and quadruple PQDs. The disadvantage is that the training time is greater. The kernel type and performance depend heavily on the type, quality, and quantity of data. For instance, a purely synthetically trained classifier may prefer an RBF kernel over a polynomial kernel, which performs better with various PQD data types. The most appropriate MSVM method, as highlighted by previous literature [23], is the one vs one (OvO) method compared to one vs all (OvA) or directed acyclic graph (DAG) for PQD classification. In OvA, a single binary SVM is trained for each PQD class, and prediction occurs on the highest confidence level. In contrast, in the OvO method, a binary SVM is trained for every PQD class pair in the dataset. During classification, the input is compared to each trained PQD model, and the output is the PQD class predicted by most models. The OvO method is used in this research and has distinct advantages when considering cost-sensitive classification.

E. MISCLASSIFICATION COSTS (MC)

The concept of MC is introduced in this paper in the process of classifying PQDs. The cost or loss associated with erroneously classifying a data point in an ML algorithm is the MC and has been widely used in the field of medicine [45]. MC varies between PQD classes since the objective is to predict one of the multiple possible classes for each sample.

PQDs that pose the most risk can cause substantial damage to electrical equipment or interrupt the power infrastructure. High-risk PQDs include voltage sags, swells, voltage spikes, and interruptions. Lower MC risks include harmonic distortions, which can cause overheating and damage to transformers, and voltage flicker, which can interfere with the functioning of sensitive industrial control systems. These are considered low-risk PQDs for MC because they are not an immediate threat and are usually compensated for after a period of PQ monitoring with either capacitor banks or with active dynamic filters (ADFs), for instance.

For better understanding, the cost of mistakenly classifying a high-risk data point, such as harmonics with sag, into a low-risk class, such as harmonics only, will increase the MC. Considering these costs, it is possible to tune the ML algorithm to reduce the MC by adjusting the weights of each type of PQD class. This is accomplished by adjusting the algorithm's parameters, such as the regularization strength, feature set, and classifiers MC to find the equilibrium between MC and OCA. The proposed DWT-CMSVM method has been weighted towards MC classes that are high-risk.

Different DSOs will have different goals when it comes to PQ indices. For example, in our method, the classification is weighted towards the sag and swell component and their subsequent related subclasses. Thus, the MC value will be closer to zero than previous literature for these PQD classes. This indicates that high-risk misclassifications (non-related PQD subclasses) are minimized.

The multiclass MC formulas below differ from the conventional method of calculating MC, in that it considers MC of unrelated PQD classes and not all misclassifications.

CA is the cost matrix (1) associated with misclassifying a sample from the true or predicted PQD class.

$$CA = \begin{array}{c} \\ \text{True Class} \end{array} \overset{\text{Predicted Class}}{\begin{bmatrix} TP_{11} & FN_{12} & FN_{i,j} \\ FP_{2,1} & TP_{22} & FN_{i,j} \\ FP_{i,j} & FP_{i,j} & TP_{i,j} \end{bmatrix}} \tag{1}$$

For cost values:

- $TP_{i,j}$: True Positive
- $FN_{i,j}$: False Negative
- $FP_{i,j}$: False Positive

After defining individual costs for $FN_{i,j}$ and $FP_{i,j}$ then the MC for a specific PQD class i and related subclasses can be calculated by (2). Here, a lower MC_i value indicates that high-risk misclassification is minimized for PQD Class i.

$$MC_i = \frac{\sum [CA(i,j) * CM(i,j)]}{n} \tag{2}$$

where:

- MC_i is misclassification cost for PQD class i
- $CA_{i,j}$ is the summation of costs that are *not* related to Class i in the CA matrix.
- $CM_{i,j}$ is the confusion matrix
- n is the total number of samples in the dataset.

III. SYNTHETIC AND REAL PQD DATA

As shown in Table 2, the previous literature was limited to laboratory/experimental, simulation, or old/limited legacy field PQD datasets [100]. Consequently, previous literature has not evaluated their methods with both synthetic and large streams of high-quality real PQ field events from modern instrumentation with higher accuracy and sampling rates.

To avoid overfitting, it is important to have a high variance of PQD data segmented and normalized for training and testing [101]. This paper contains 29 PQD classes, including 13 standard and 16 complex classes.

A. SYNTHETIC PQD DATASET

For synthetic data generation, the duration, starting and ending time of each PQD class is varied randomly within appropriate parameters to avoid overfitting.

The synthetic data of standard and complex PQD classes and case numbers evaluated in this paper is shown in Table 3 and was adapted from previous literature [101] and IEEE standards.

TABLE 2. Measurement Data, Pre-processing, and Feature Extraction Characteristics of Previous Literature and Proposed Method.

Stage	Measurement Data					Pre-processing			Features Extraction	
Data Type	Synthetic			Real Field						
Attribute	Lab	Simulation	Model	Legacy	Modern	Segmentation	Denoise	Normalization	Crafted	Algorithm
Ref.	[3, 14, 18, 22, 36, 41, 44, 52-71]	[3, 8, 14, 19, 23, 37, 38, 52, 69, 72-87]	[16, 18, 19, 22, 23, 36, 37, 39-42, 44, 53-61, 63-67, 69, 70, 72, 76-78, 81, 85, 87-98]	[3, 22, 33, 38, 43, 68, 74, 76, 79, 87, 92, 96, 99]		[8, 16, 22, 33, 37-44, 54, 60, 62, 69-73, 77, 82, 85, 87, 90, 91, 99]	[36-38, 57, 70, 71, 80, 92]	[14, 18, 23, 33, 37-44, 57, 58, 60-62, 64, 67, 68, 73, 75-79, 81-89, 93-95, 97-99]	[3, 8, 14, 16, 18, 22, 23, 36, 38, 42, 52, 53, 55-63, 65, 67, 68, 70, 72-75, 77-84, 86-92, 95-99]	[19, 37, 39-41, 43, 44, 66, 80, 93, 94]
Proposed	✓	✓	✓		✓	✓	✓	✓	✓	
Notes	Lab: laboratory or experimental. Simulation: simulated PQD scenarios. Model: dataset generated from mathematical formulae, Real Field Data: Legacy – small and/or old dataset with low sampling rate from legacy instruments such as transmission level PMUs or older PQAs. Modern – larger dataset from new technology such as modern PQAs, DFRs, or μPMUs with higher accuracy and high-sampling rate above 256 samples/cycle. Segmentation: relevant events isolated for training and testing. Denoise: noise filtering algorithm. Normalization: conversion to specific scale. Feature Extraction: Crafted – specific features selected. Algorithm: automatically selected features									

B. REAL FIELD DATASET

The uniqueness of this study is that real field data will be used to train and test the algorithm. μPMU manufacturers have embedded PQA abilities in their instruments. However, due to the lack of accessible real synchrophasor field data in Australia, real-world data from PQAs will be used. This field dataset is limited to only 13 standard PQDs because complex PQDs occurred far less in the field (later discussed in limitations).

Elspec's PQSCADA Sapphire Software was used to segment and export the PQ field events, which contain over a decade's worth of continuous historical recording from different projects in Australia, including distribution feeders, large-scale industrial projects, renewables, airports, production plants, hospitals, and more. The PQ data from the Elspec G4430/G4500 [102] is compliant with standards EN50160, IEEE519, IEC-61000-4-30 and has a voltage sampling rate of 512 samples/cycle (20ms), similar to μPMU reporting rate of 50 frames per second. The Elspec G5DFR, G5PMU [47], G4500, and PureBB was also used.

Fig. 2-6 show examples of real PQD field data used in this research including parameters used in the proposed feature set.

C. DATA WINDOW, SAMPLING RATE, AND LATENCY

In accordance to the IEEE standard [103], the PQ sampling window is set at ten cycles at 50Hz. Table 4 shows the sampling rate and its effect on the performance of the proposed method for standard PQDs. This aspect has not been explored in previous literature. Deteriorated performance occurs at 128 samples/cycle due to the boundary effects of wavelet decomposition after seven levels, but adequate performance at 256 samples/cycle. The recommended instrument sampling rate is 512 or 1024 samples/cycle for the proposed method.

Moreover, additional laboratory tests were conducted from the Elspec G4430 PQA [102] to a Raspberry Pi (single phase μPMU). The latency is 18ms using standard Modbus protocol and 6-8ms using priority Modbus for cyclic measurements. This makes the proposed method suitable for real-time and critical applications considering fault ride-through (FRT) requirements.

TABLE 3. Cases of Standard and Complex PQDs.

Case	Standard PQDs	Case	Complex PQDs
C01	Pure Signal	C14	Sag + Oscillatory Transient
C02	Sag	C15	Swell + Oscillatory Transient
C03	Swell	C16	Sag + Harmonics
C04	Interruption	C17	Swell + Harmonics
C05	Transient	C18	Harmonics + Sag + Flicker
C06	Oscillatory Transient	C19	Harmonics + Swell + Flicker
C07	Harmonics	C20	Sag + Harmonics + Flicker
C08	Harmonics + Sag	C21	Swell + Harmonics + Flicker
C09	Harmonics + Swell	C22	Sag + Harmonics + Oscillatory Transient
C10	Flicker	C23	Swell + Harmonics + Oscillatory Transient
C11	Flicker + Sag	C24	Harmonics + Sag + Oscillatory Transient
C12	Flicker + Swell	C25	Harmonics + Swell + Oscillatory Transient
C13	Notch	C26	Harmonics + Sag + Flicker + Oscillatory Transient
Notes	For this research f = 50Hz, fs = 25600Hz = 512 samples/cycle.	C27	Harmonics + Swell + Flicker + Oscillatory Transient
		C28	Sag + Harmonics + Flicker + Oscillatory Transient
		C29	Swell + Harmonics + Flicker + Oscillatory Transient

As exemplified in earlier sections, there are two optimal choices for the choice of decomposition level. Firstly, if accuracy is the priority, an eight-level decomposition is recommended. Secondly, if speed is the priority or the computational burden is too high due to the hardware limitations, then a four-level decomposition method is recommended for faster computation with satisfactory OCA results, as shown in Fig. 1.

Another factor that dictates which decomposition is suitable is the sampling rate. If a low sampling rate is used with the proposed method, then there are marginal gains in OCA after four-level decomposition, as discussed in Section II.

It is also important to note that transmission delay, which can be tens of milliseconds, is not considered since it varies by protocol and hardware variance.

This research used an eight-level decomposition level to achieve the best OCA with a high-sampling rate for all case

TABLE 4. Instrument Sampling Rate vs OCA.

Sampling Rate (Hz)	Samples / Cycle	OCA (%)
6400	128	94.38
12800	256	95.92
25600	512	98.35
51200	1024	98.35

studies. For the proposed method, when standard PQD cases are considered, the computational time is a minimum of 48ms without the noise filter, to a maximum of 84ms with the noise filter. The proposed method is still computationally efficient at eight-levels of decomposition with high-sampling rates, and under the PQ sliding window of 10 cycles (200ms).

IV. PROPOSED PQD CLASSIFICATION METHODOLOGY

By considering all the attributes discussed in earlier sections, an improved DWT-CMSVM PQD classification method is presented, as shown in Fig. 7. The number and benefit of all DWT features have been extensively discussed in previous literature [29]. After experimenting with all the features, an optimal set of features was handcrafted for evaluation in this paper for efficiency improvements. In addition to μPMU voltage synchrophasors, the DWT feature vectors include RMS, Shannon's entropy, energy, mean value, max percentage, and approximate and detailed coefficients. In addition, THD and instantaneous flicker measurement as additional features are used in the extraction process. This is new and unseen from previous literature [16], [19], [27], [29], [33], [104] using the DWT method. All values are normalized.

A. DWT MATHEMATICAL FORMULATION

The different versions of the original signal are represented by the detailed coefficients and approximate coefficients. The best standard DWT feature set for eight-level decomposition is shown in [19] in addition to the new ones presented in this paper.

$$DWT_f^{\psi}(j,k) = \frac{1}{\sqrt{a_0^j}} \sum_{n=-\infty}^{\infty} f(n)\, \psi \left[\frac{n - a_0^j k b_0}{a_0^j} \right] \tag{3}$$

where: $j, k, n \in Z$ *and* $a_0 > 1$ *and* $\psi\left(\frac{t}{s}\right) s > 0$

The DWT discretized wavelet is:

$$\psi_{j,k}(t) = \frac{1}{\sqrt{2^{\frac{j}{v}}}} \psi \left(\frac{t - k2^{\frac{j}{v}}}{2^{\frac{j}{v}}} \right) dt \tag{4}$$

where: *scaling parameter* $j \in z$, *time shifting parameter* $k \in z$, *voices per octave* $v = 1$

MRA is performed using a wavelet transform that produces approximate and detailed coefficients to extract the following features.

B. SHANNON'S ENTROPY

Shannon's Entropy

$$SE_i = -\sum_{j=1}^{N} S_{i,j}^2 log\left(S_{i,j}^2\right) \tag{5}$$

$S_{i,j}$ *is the orthonormal coefficents of the original signal S.*

Entropy Approximate

$$\phi_i = 2^{\frac{i}{2}} \sum_{j=1}^{N} c_{j,n} \phi \left[2^j t - n \right] \tag{6}$$

Entropy Detailed

$$\psi_{j,n} = 2^{\frac{j}{2}} \sum_{j=1}^{N} c_{j,n} \psi \left[2^j t - n \right] \tag{7}$$

C. COEFFICIENT ENERGY, MAX PERCENTAGE, MEAN VALUE

Coefficient Energy

$$CE = \sum_{j=1}^{N} |S_{i,j}|^2 \tag{8}$$

Max Percentage of Detailed Coefficients

$$MP = \sum_{j=1}^{N} |D_{i,j}|^2 \tag{9}$$

Mean Value of Detailed Coefficients

$$\mu_i = \frac{1}{N} \sum_{j=1}^{N} (D_{i,j}) \tag{10}$$

D. ROOT MEAN SQUARE (RMS)

$$RMS_i = \sqrt{\frac{1}{N} \sum_{j=1}^{N} C_{i,j}^2} \tag{11}$$

E. TOTAL HARMONIC DISTORTION (THD)

$$THD\,(\%) = \frac{\sqrt{\sum_{n=2}^{\infty} V_{nrms}^2}}{V_{rms}}.100 \tag{12}$$

F. INSTANTANEOUS FLICKER

Flicker has been neglected in previous studies in feature selection, especially when differentiating complex PQD classes. The flicker phenomenon is non-linear and is initiated by sudden load changes making it difficult to incorporate into any method. Thus, a flicker meter to measure instantaneous flicker (Pfs), short-term flicker (Pst), and long-term flicker (Plt) was developed in MATLAB compliant with the IEEE 1453-2015 standards [105]. The Pfs and Pst indices can be used for real-time classification, whereas the Plt can be used for long term view of PQ over the 120 min period. The Pfs measurement is normalized over the sampling window of 10 cycles.

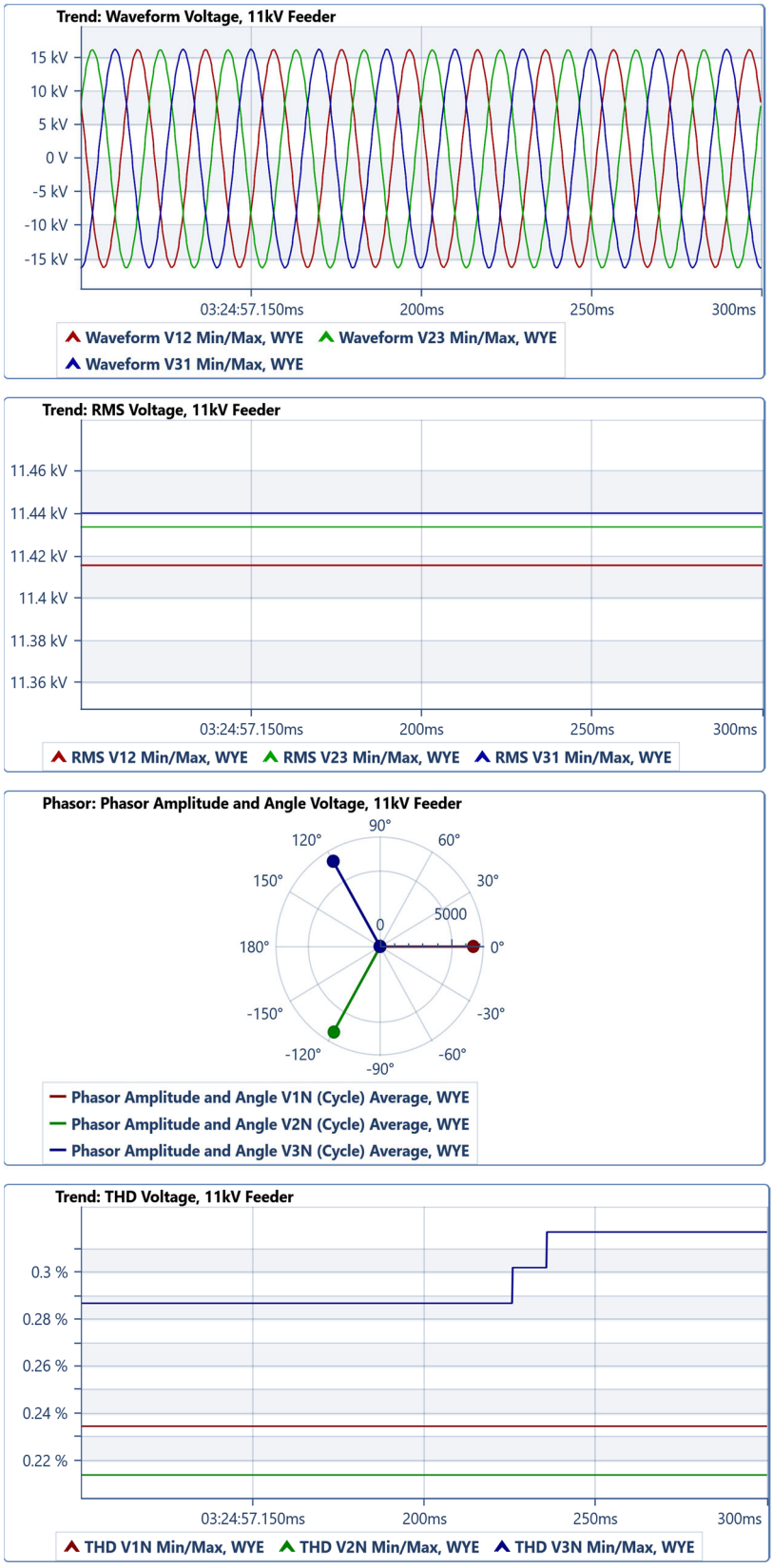

FIGURE 2. Normal PQD Condition - Real Field Data - 11kV Australian Distribution Feeder: Continuous L-L Voltage Waveform, RMS Voltage, Magnitude and Angle Voltage Phasors, THD Voltage.

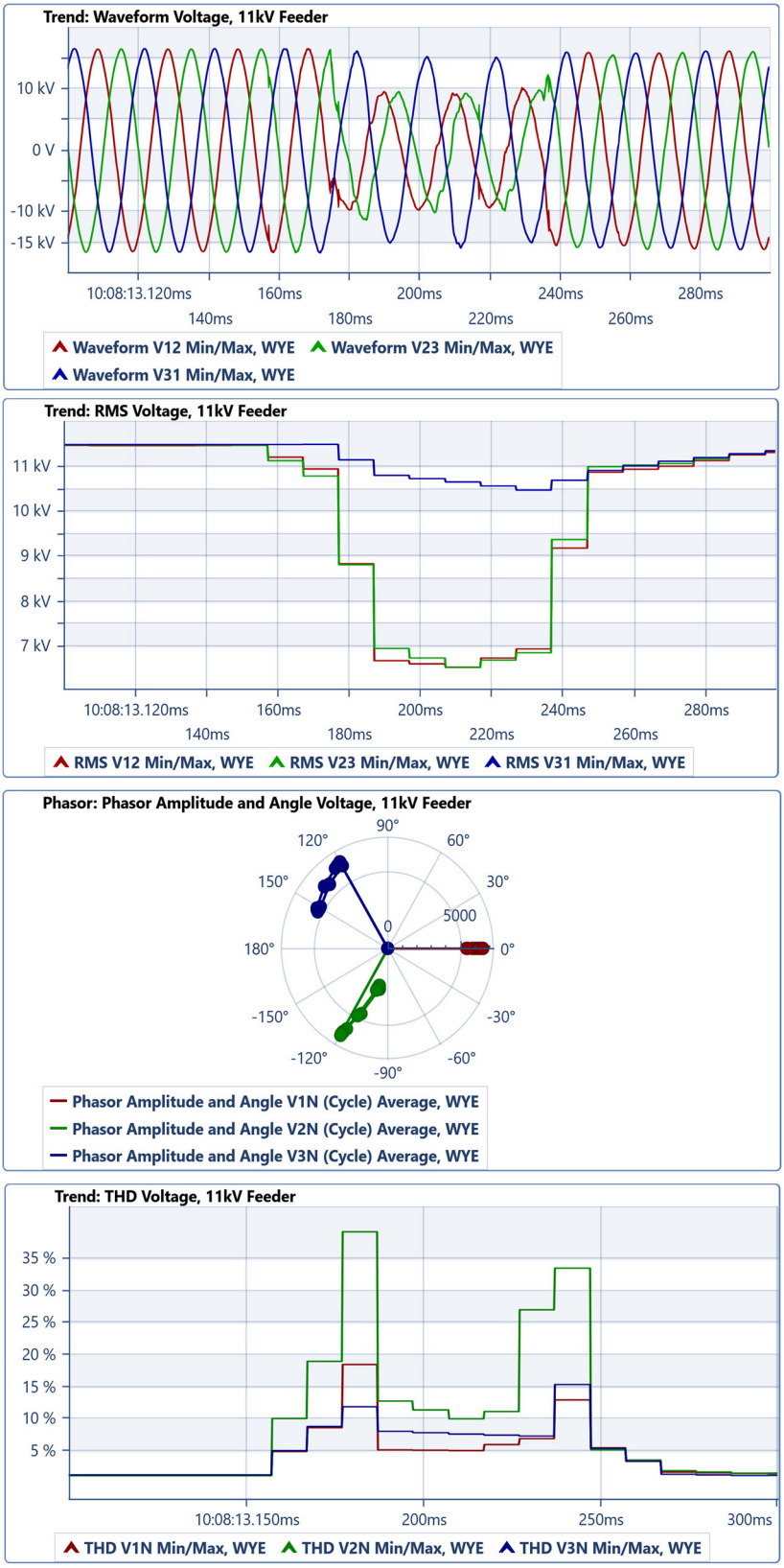

FIGURE 3. Sag PQD Condition – Real Field Data - 11kV Australian Distribution Feeder: Continuous L-L Voltage Waveform, RMS Voltage, Magnitude and Angle Voltage Phasors, THD Voltage.

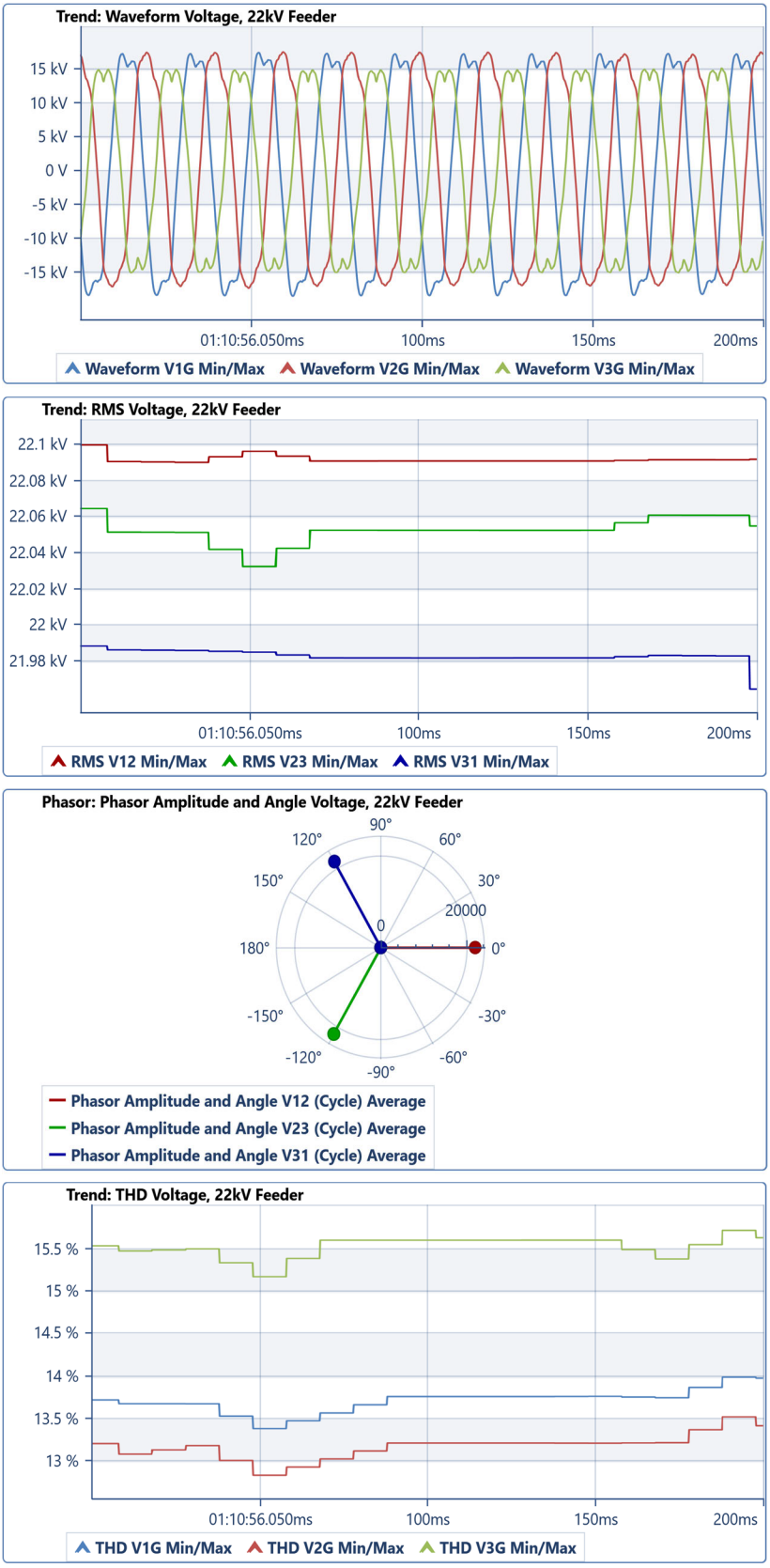

FIGURE 4. Harmonics PQD Condition – Real Field Data - 22kV Australian Distribution Feeder: Continuous L-G Voltage Waveform, RMS Voltage, Magnitude and Angle Voltage Phasors, THD Voltage.

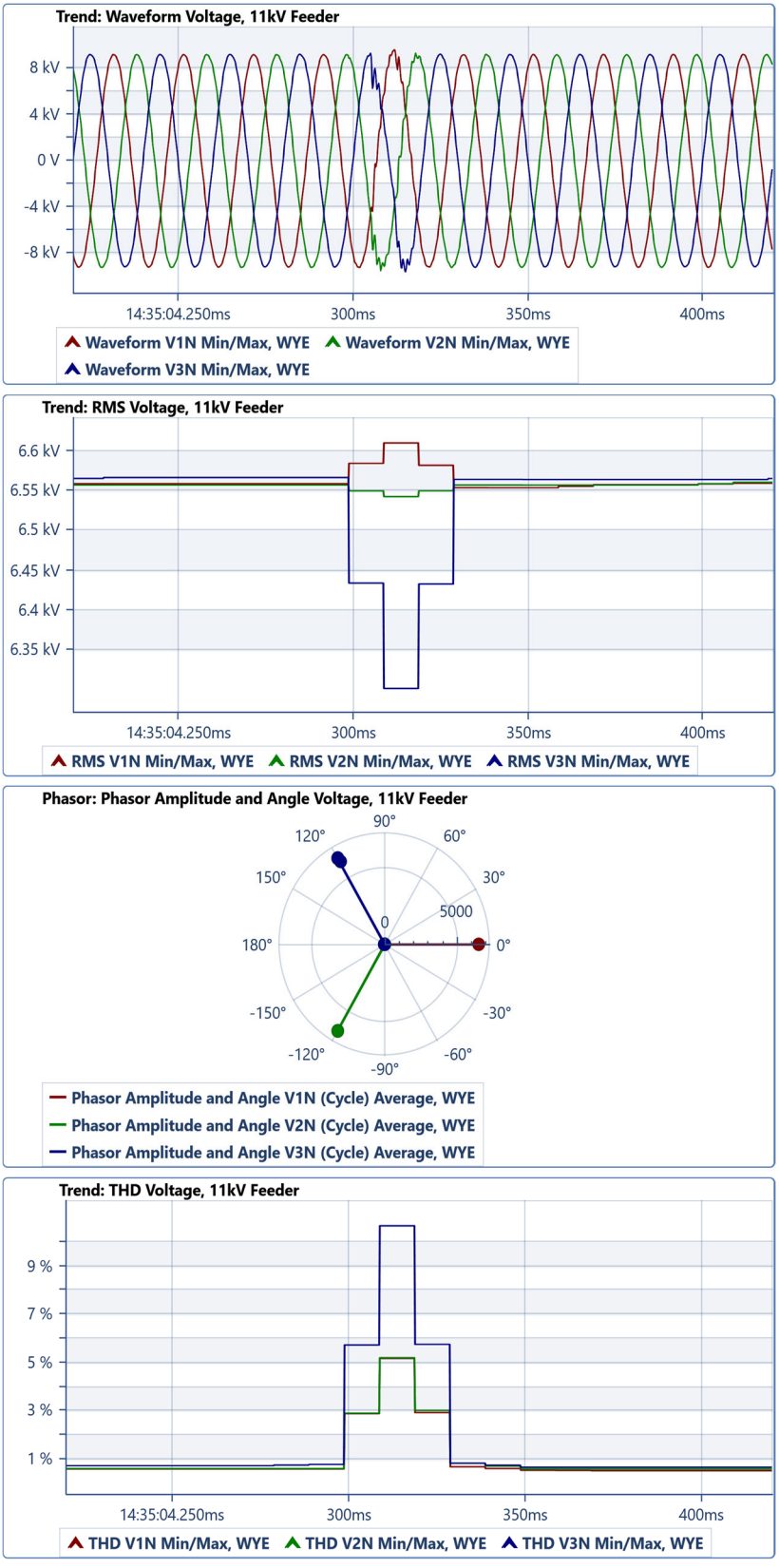

FIGURE 5. Normal and Harmonics PQD Condition – Real Field Data - 11kV Australian Distribution Feeder: Continuous L-G Voltage Waveform, RMS Voltage, Magnitude and Angle Voltage Phasors, THD Voltage.

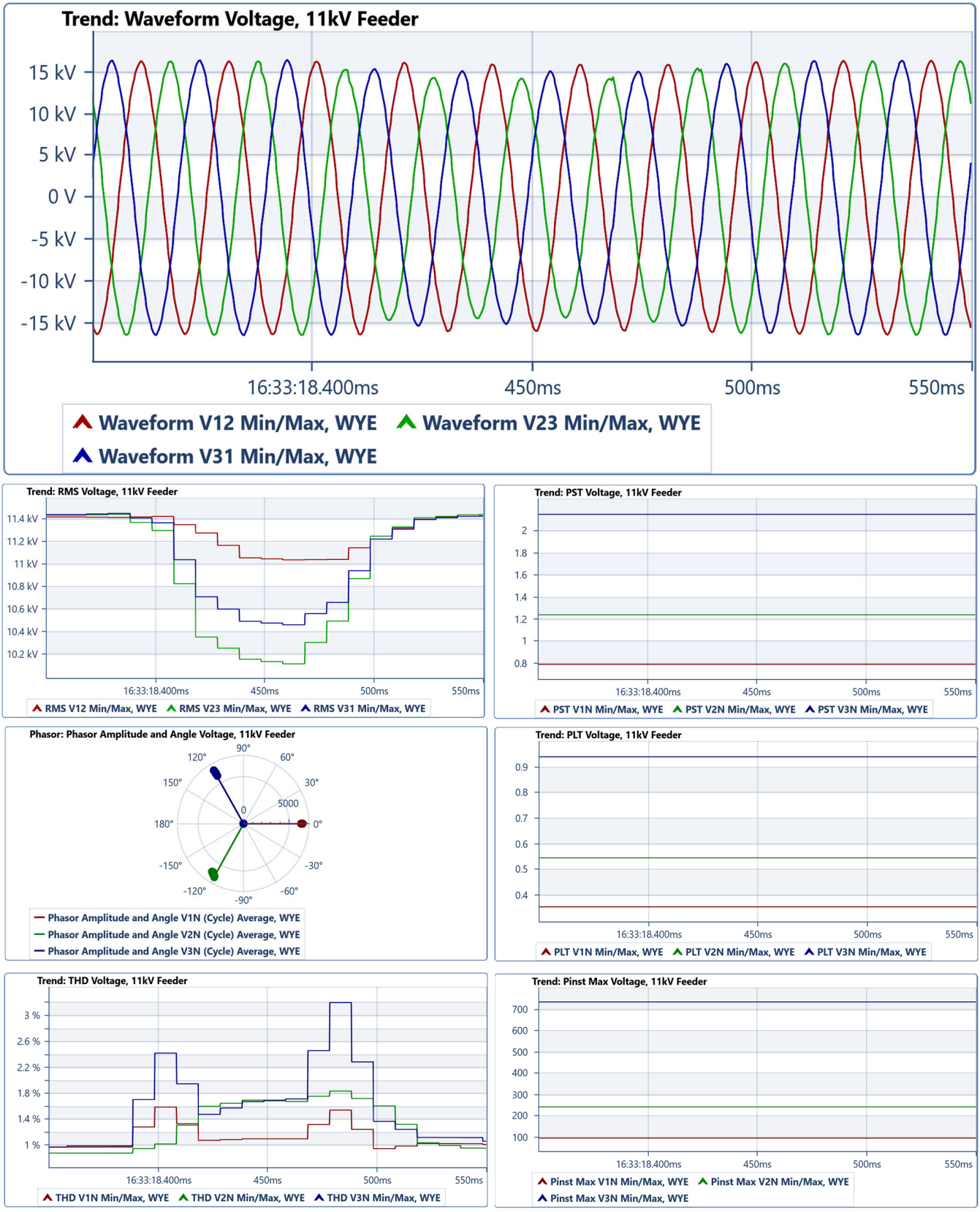

FIGURE 6. Flicker PQD Condition – Real Field Data - 11kV Australian Distribution Feeder: Continuous L-L Voltage Waveform, RMS Voltage, Magnitude and Angle Voltage Phasors, THD Voltage, Short-Term PST Voltage Flicker, Long-Term Voltage Flicker PLT, Instantaneous Voltage Flicker.

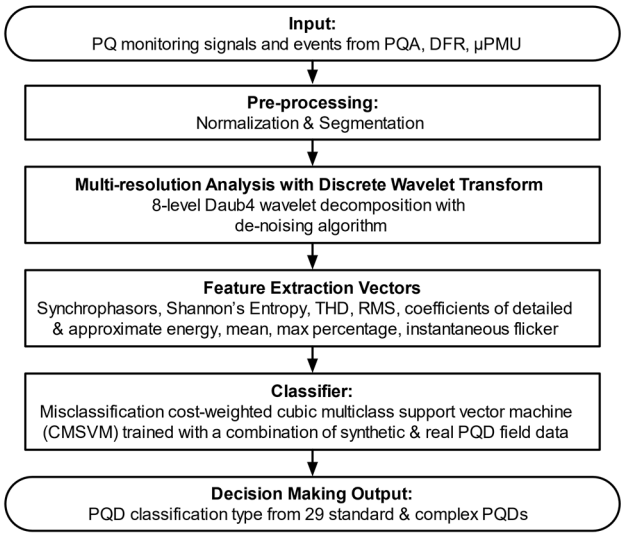

FIGURE 7. Simplified Flowchart of Proposed DWT-CMSVM Method.

TABLE 5. Case Study Overview.

	PQD Type	# of PQDs	Training Type & Number		Testing Type & Number	
Case Study 1	Standard	13	Synthetic	200	Synthetic	200
Case Study 2	Standard	13	Synthetic	200	Real	200
Case Study 3	Standard	13	Synthetic	100	Synthetic	100
			Real	100	Real	100
Case Study 4	Standard Complex	29	Synthetic	800	Synthetic	800
			Real	200	Real	200

G. DISTINCTIVE FEATURE CHARACTERISTICS CONSIDERING MC

The distinctive feature characteristics to show the MC-weighted classification are shown in Fig. 8 for standard PQDs. The most likely source of misclassification will occur at overlapping features, and the objective is to minimize MC. For instance, if harmonics with sag is misclassified, it will most likely be misclassified as flicker with sag and not flicker only, thus lowering MC risk.

The proposed method has no problem classifying high-frequency fluctuations such as notching since it has a unique mean energy characteristic and will not overlap with other features. As a result, classes with unique feature characteristics are less likely to be misclassified.

V. RESULTS AND DISCUSSION

Case studies evaluated in this paper are shown in Table 5, including PQD type, training, and testing signal splits. While synthetically generated data can be increased to any number, it has been limited to maintain between 20-50% of real field PQD data.

A. CASE STUDY 1 – SYNTHETIC VS. SYNTHETIC

The results for Case Study 1 are shown in Table 6 when the proposed DWT-CMSVM method is trained and tested on synthetic data only. The diagonal elements of a confusion matrix represent the correctly classified PQDs, whereas the

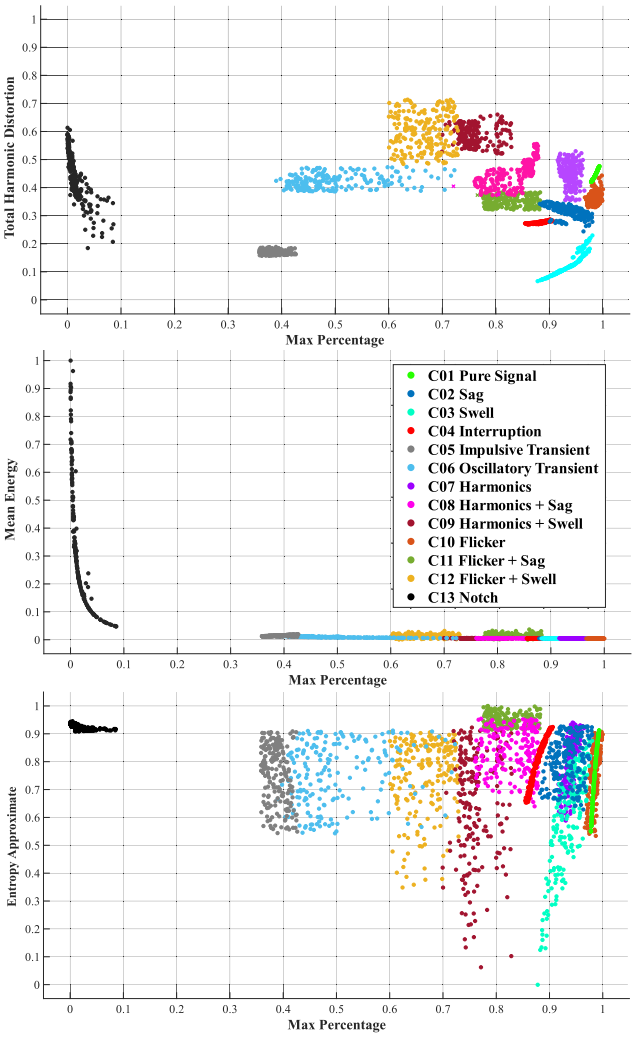

FIGURE 8. Distinctive Feature Characteristics considering Misclassification Costs: Max Percentage vs THD (top), Mean Energy (middle), and Entropy Approximate (bottom).

off-diagonal elements represent misclassifications. Empty elements represent a zero value for readability.

Notable points from Case Study 1

- C06 oscillatory transient was misclassified once as C10 flicker and C01 pure
- C10 flicker was classified as C01 pure once
- C11 flicker with sag was classified as C02 sag once, and C08 harmonics with sag twice
- Similarly, there was one instance where C12 flicker with swell was classified C03 swell, and twice as C09 harmonics with swell.

The high OCA of 99.65% is in-line with all previous studies using synthetically trained and tested datasets. In terms of MC, it is safer for any method to misclassify C11 and C12 as C02-03 or C08-09, respectively. This is because voltage sag, swells, and interruptions are at higher MC risk than flicker alone, especially for real-time control. The proposed method has a pattern and tendency to correctly classify sag and swells with more weight than other PQDs. This highlights the importance of selecting the right feature set and optimizing the OvO

TABLE 6. Case Study 1 - Confusion Matrix.

True Class	Predicted Class													
	C01	C02	C03	C04	C05	C06	C07	C08	C09	C10	C11	C12	C13	Accuracy
C01	200													100.00
C02		200												100.00
C03			200											100.00
C04				200										100.00
C05					200									100.00
C06	1					198				1				99.00
C07							200							100.00
C08								200						100.00
C09									200					100.00
C10	1									199				99.50
C11		1						2			197			98.50
C12			1						2			197		98.50
C13													200	100.00
Overall Classification Accuracy: 99.65%														

TABLE 7. Case Study 2 - Confusion Matrix.

True Class	Predicted Class													
	C01	C02	C03	C04	C05	C06	C07	C08	C09	C10	C11	C12	C13	Accuracy
C01	197	3												98.50
C02	4	196												98.00
C03	2		198											99.00
C04		5		195										97.50
C05	6		3		191									95.50
C06	5					189			2	2		2		94.50
C07							193	5	2					96.50
C08	2	4						194						97.00
C09			3				2		195					97.50
C10	7					2				186	3	2		93.00
C11		4								3	191	2		95.50
C12			4							4	1	191		95.50
C13	2												198	99.00
Overall Classification Accuracy: 96.70%														

CMSVM classifier through cost weights during the training stage, as previously discussed and shown in Fig. 8.

B. CASE STUDY 2 – SYNTHETIC VS. REAL

Table 7 highlights the importance of using field PQDs in any classification method. Here, the DWT-CMSVM was trained only on synthetically generated signals and tested on real field data. The OCA significantly dropped from 99.65% to 96.70%. Overall, there is a severe deterioration in OCA and increased risk in MC when tested on real PQDs.

Notable Points from Case Study 2

- C01 pure was misclassified as C02 sag three times
- C02 sag was misclassified as C01 pure four times, with C03 swell misclassified as C01 pure twice
- C04 interruption was misclassified as C03 sag
- C05 transient was misclassified six times as C01 pure and swell three times
- C06 oscillatory transient was misclassified as C01 pure five times; C10 flicker, C12 flicker with swell, and C09 harmonics with swell twice each
- C08-C09 harmonics related sag and swell were misclassified favourably as C02-C03 to minimize MC
- MC for C10-C12 flicker sag/swell-related PQDs are much higher than in Case Study 1. It is preferred to classify these as sag related C02/C08 and swell related C03/C09 swell, respectively, to lower MC risk.
- C10 flicker was misclassified as C01 pure seven times, C11 flicker with sag three times, and, C12 flicker with swell twice. A similar situation occurs with C11-C12 flicker with sag and swell related distortions.
- Higher frequency energy components such as C05 transients and C13 notching had OCAs of 95.50% and 99.00%, respectively.

TABLE 8. Case Study 3 - Confusion Matrix.

True Class	Predicted Class													
	C01	C02	C03	C04	C05	C06	C07	C08	C09	C10	C11	C12	C13	Accuracy
C01	200													100.00
C02	3	197												98.50
C03	2		198											99.00
C04		3		197										98.50
C05			4		196									98.00
C06	4					194				2				97.00
C07							198	2						99.00
C08							2	197	1					98.50
C09			2				1		196			1		98.00
C10	4									193	2	1		96.50
C11		2						2			196			98.00
C12			2						3			195		97.50
C13													200	100.00
Overall Classification Accuracy: 98.35%														

C. CASE STUDY 3 – SYNTHETIC/REAL VS. REAL

In Case Study 3, OCA improved by 1.65% over the previous case study, alongside valuable enhancements to MC, as depicted in Table 8. Here, the proposed DWT-CMSVM method is trained and tested with an even combination of synthetic and field PQDs.

However, the OCA is still substantially lower than purely synthetic Case Study 1. In the only other literature of this kind, authors in [34] achieved similar improvements to their MSVM classifier for five basic PQDs, when it was trained on a combination of data from a real power network and synthetic data.

Notable Points from Case Study 3

- OCA is worse than Case Study 1, and highlights the importance of using high-quality field data
- Variations in MC with better performance compared to Case Study 2. This phenomenon is seen through

TABLE 9. Case Study 4 - Confusion Matrix - Heat Map.

True Class \ Predicted Class	1	2	3	4	5	6	7	8	9	10	11	12	13	14	15	16	17	18	19	20	21	22	23	24	25	26	27	28	29
1	1000	0	0	0	0	0	0	0	0	0	0	0	0	0	0	0	0	0	0	0	0	0	0	0	0	0	0	0	0
2	0	1000	0	0	0	0	0	0	0	0	0	0	0	0	0	0	0	0	0	0	0	0	0	0	0	0	0	0	0
3	0	0	1000	0	0	0	0	0	0	0	0	0	0	0	0	0	0	0	0	0	0	0	0	0	0	0	0	0	0
4	0	0	0	1000	0	0	0	0	0	0	0	0	0	0	0	0	0	0	0	0	0	0	0	0	0	0	0	0	0
5	0	0	0	0	1000	0	0	0	0	0	0	0	0	0	0	0	0	0	0	0	0	0	0	0	0	0	0	0	0
6	4	0	0	0	0	980	0	0	0	0	9	4	0	0	0	0	0	1	2	0	0	0	0	0	0	0	0	0	0
7	0	0	0	0	0	0	1000	0	0	0	0	0	0	0	0	0	0	0	0	0	0	0	0	0	0	0	0	0	0
8	0	0	0	0	0	0	0	991	0	0	0	0	0	0	0	6	0	3	0	0	0	0	0	0	0	0	0	0	0
9	0	0	3	0	0	0	0	0	993	0	0	0	0	0	0	0	4	0	0	0	0	0	0	0	0	0	0	0	0
10	5	0	0	0	0	0	0	0	0	995	0	0	0	0	0	0	0	0	0	0	0	0	0	0	0	0	0	0	0
11	0	0	0	0	0	0	0	0	0	0	982	0	0	0	0	0	0	13	0	5	0	0	0	0	0	0	0	0	0
12	0	0	6	0	0	0	0	0	0	0	0	980	0	0	0	0	0	0	9	0	5	0	0	0	0	0	0	0	0
13	0	0	0	0	0	0	0	0	0	0	0	0	1000	0	0	0	0	0	0	0	0	0	0	0	0	0	0	0	0
14	0	0	0	0	0	0	0	0	0	0	0	0	0	963	0	0	0	3	0	5	0	11	0	4	0	5	0	9	0
15	0	0	0	0	0	2	0	0	0	0	0	0	0	0	969	0	0	0	0	0	0	0	18	0	3	0	3	0	5
16	0	0	0	0	0	0	0	0	0	0	0	0	0	0	0	961	0	6	0	0	0	18	0	0	0	15	0	0	0
17	0	0	0	0	0	0	0	0	0	0	0	0	0	0	0	0	956	10	0	21	0	0	0	1	0	5	0	0	7
18	0	0	0	0	0	0	0	23	0	0	26	0	0	0	0	0	0	810	0	77	0	0	0	5	0	55	0	4	0
19	0	0	0	0	0	0	1	0	1	0	0	14	0	0	0	0	32	0	832	0	41	0	0	0	14	0	53	0	12
20	0	0	0	0	0	0	0	4	0	0	0	0	0	0	0	0	24	8	122	0	824	0	3	0	5	0	7	0	3	0
21	0	0	3	0	0	0	0	0	4	0	0	0	0	0	0	0	118	0	81	0	783	0	3	0	5	0	1	0	2
22	0	0	0	0	0	0	0	3	0	0	0	0	0	37	0	30	0	11	0	35	0	831	0	15	0	13	0	25	0
23	0	0	0	0	0	2	0	0	5	0	0	0	0	0	35	0	41	3	9	0	15	0	796	0	45	6	21	0	22
24	0	0	0	0	0	0	0	0	0	0	0	0	0	18	0	6	0	0	0	8	0	72	0	788	0	34	4	68	2
25	0	0	0	0	0	6	0	0	0	0	0	0	0	0	13	0	8	0	0	2	5	0	81	0	803	7	24	0	51
26	0	0	0	0	0	0	0	0	0	0	4	0	0	28	0	4	7	78	3	7	0	34	0	0	7	789	0	39	0
27	0	0	0	0	0	3	0	0	0	0	0	0	0	0	9	0	11	0	93	0	23	0	11	0	70	0	763	0	17
28	0	0	0	0	0	0	0	0	0	0	5	0	0	12	0	3	0	7	0	49	0	24	0	53	0	92	0	755	0
29	0	0	0	0	0	11	0	0	0	0	0	8	0	0	12	0	19	0	16	0	52	0	36	2	34	0	39	0	771

appropriate misclassification of C04 interruption as C02 sag three times and C05 transient as C03 swell four times.

- The proposed method has trouble classifying field C06 oscillatory transients, namely as C11-C12 flicker-related sag and swell, as shown in Fig. 8. This is a disadvantage of using fixed wavelet size in DWT compared to variable wavelet sizes in CWT.
- In Case Study 2, C11 flicker with sag was misclassified as C10 flicker. Here, it has been classified as sag-related distortions C02 and C08 harmonics with sag, reducing the MC.
- There are instances of C12 flicker with swell classified as C03 swell or C09 harmonics with swell. The misclassifications are not entirely incorrect and improve MC compared to the previous Case Study.

D. CASE STUDY 4 – SYNTHETIC/REAL VS. SYNTHETIC/REAL

The results of Case Study 4 are shown in Table 9 heatmap. Using the proposed DWT-CMSVM method, 800 synthetically generated signals and 200 standard field PQDs were trained and tested with different datasets. As previously discussed, due to the lack of a large stream of complex field PQDs, only Cases C01-C13 have been trained on a combination of real and synthetic PQDs, whereas, Cases C14-C29 have been purely synthetically trained and tested. The synthetic data has been limited to 800, to maintain at least 20% of real field data.

Notable points from Case Study 4

- The OCA performance significantly dropped from 98.35% to 90.74% when the proposed technique was evaluated with 29 standard and complex PQDs.
- The method performs the best for Cases C01-C13, shows moderate performance between C14-C17, and degraded performance when faced with triple and quadruple PQDs from C18-C29.
- PQD cases C18-C29 averaged 79.54% classification accuracy. While this number is lower than in previous case studies, the incorrectly classified cases have favorable MC as shown in Table 9.
- For example, C18 (harmonics with sag with flicker) was favorably misclassified as C11 (flicker with sag) or C26 (harmonics with sag with flicker with oscillatory transient).
- However, there were 77 instances where C18 (harmonics with sag with flicker) was misclassified as C20 (sag with harmonics with flicker). A similar pattern is seen in all subsequent complex PQD cases to varying extents. Traditional ML methods will have trouble distinguishing between these.
- C19 (harmonics with swell with flicker) was favorably misclassified mainly as C26 (harmonics with swell with flicker with oscillatory transient)
- A greater spread of incorrect classification cases exists in other cases, such as C22/C23 (sag/swell with harmonics with oscillatory transient).
- However, the sag/swell component for which the proposed method is weighted indicates low-risk MC, which is more valuable than entirely incorrect classifications.
- Due to their unique energy high-frequency notching components can be detected confidently.
- With only a few exceptions, this trend for the proposed method to misclassify more complex PQDs (C14-C29) to lower MC is favorable compared to previous literature.

VI. APPLICATION CASE STUDIES

The following section presents five unique application case studies highlighting how the proposed PQD classification method can be used with an optimal μPMU placement

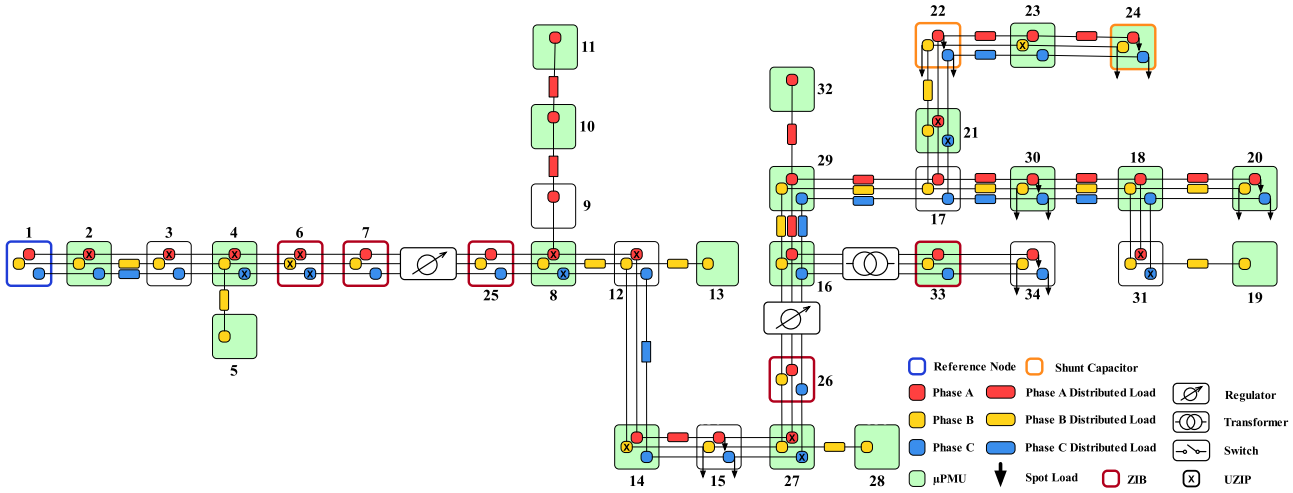

FIGURE 9. Optimal Placement of μPMU in IEEE-34 Distribution Test System using UZIP String algorithm [51].

TABLE 10. Application Case Study 1 - Line-to-Line Fault – Phase B and Phase C - IEEE-34 Distribution Network with Optimally Placed μPMUs.

Node	16 μPMU		Node	33 μPMU	
Phase	Predicted	True	Phase	Predicted	True
A	C01 - Normal	✓	A	C03 - Swell	✓
B	C01 - Normal	✓	B	C02 - Sag	✓
C	C02 - Sag	✓	C	C02 - Sag	✓
OCA	100%		OCA	100%	

TABLE 11. Application Case Study 2 - Induction Motor DOL Start – IEEE-34 Distribution Network with Optimally Placed μPMUs.

Node	16 μPMU		Node	33 μPMU	
Phase	Predicted	True	Phase	Predicted	True
A	C01 - Normal	✓	A	C02 - Sag	✓
B	C01 - Normal	✓	B	C02 - Sag	✓
C	C01 - Normal	✓	C	C02 - Sag	✓
OCA	100%		OCA	100%	

TABLE 12. Application Case Study 3 – Capacitor Bank Energizing LV & HV Sides – IEEE-34 Distribution Network with Optimally Placed μPMUs.

Node	16 μPMU		Node	33 μPMU	
Phase	Predicted	True	Phase	Predicted	True
A	C06 - Oscillatory	✓	A	C06 - Oscillatory	✓
B	C06 - Oscillatory	✓	B	C06 - Oscillatory	✓
C	C06 - Oscillatory	✓	C	C06 - Oscillatory	✓
OCA	100%		OCA	100%	

scheme to provide DSOs with better PQ insights and evaluate the distribution network's overall PQ health. The optimal μPMU placement occurs at either side of the transformer at Node 16 and Node 33 as per the UZIP String optimal placement algorithm developed in [51] and shown in Fig. 9. The validated Class M μPMU model [106] is simulated in MATLAB/Simulink software with PQ studies presented in [107]. The only modifications are the 25.9 kV to 400V Delta-Wye (Dy11), 1 MVA transformer between Node 16 high-voltage (HV) side and Node 33 low-voltage (LV) side. Node 33 remains a zero-injection bus (ZIB), and the line parameters are identical to match the original IEEE-34 node test feeder design.

A. APPLICATION CASE STUDY 1 – FAULTS

A line-to-line fault between Phase B and Phase C is simulated between Node 16 and the HV side of the transformer with a high fault impedance of 50 Ω. For this example, the load is rated at 15 kW and 125 Var at Node 34. The fault starts at 1.1 seconds with a duration of 5 cycles, as shown in Fig. 10. At Node 16, Phase B on the HV side experiences a slight voltage drop and rises beyond the nominal voltage, whereas a voltage sag occurs in Phase C. In contrast, the Node 33 LV side experiences a voltage sag in Phases B and C, and a voltage swell in Phase A. The classification results per voltage channel are shown in Table 10 and achieved 100% OCA.

The voltage dip/rise experienced in Phase B on the HV side is within the IEEE standard sag/swell magnitude limits of 0.9 p.u to 1.1 p.u. The swell experienced by Node 33 Phase B is due to the high fault impedance and the nature of line-to-line fault having no ground [107]. A basic threshold-based sag/swell event detection can also be easily implemented alongside the proposed method for added PQ insights.

Another factor is the Dy11 configuration of the transformer. Here, the LV side leads the HV side, causing a +30-degree phase shift, as shown by the phase angles in Fig. 10. This will be present in subsequent case studies. An additional 72 fault scenarios were generated by altering fault type and impedances (1Ω, 25Ω, and 50Ω), achieving an OCA of 100%.

This unique application case study shows the importance of μPMU placement in its ability to pick up PQDs on either side of a transformers or automatic voltage regulators (AVRs), which are treated as unknown network parameter (UNP) by the UZIP String optimal μPMU placement method [51].

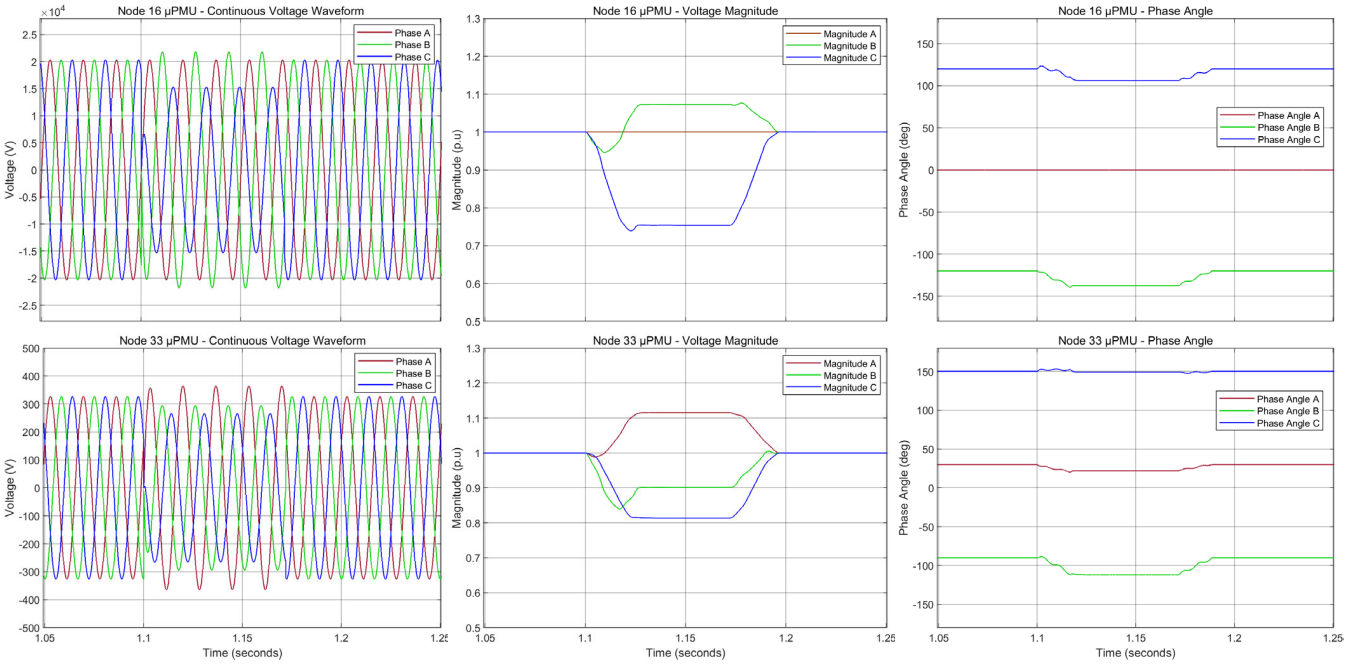

FIGURE 10. Application Case Study 1 - Line-to-Line Fault (Phase B and Phase C) - IEEE-34 Node Test Network, Node 16 μPMU (top) and Node 33 μPMU (bottom); Continuous L-G Voltage Waveform (left), Voltage Magnitude (middle), and Phase Angle (right).

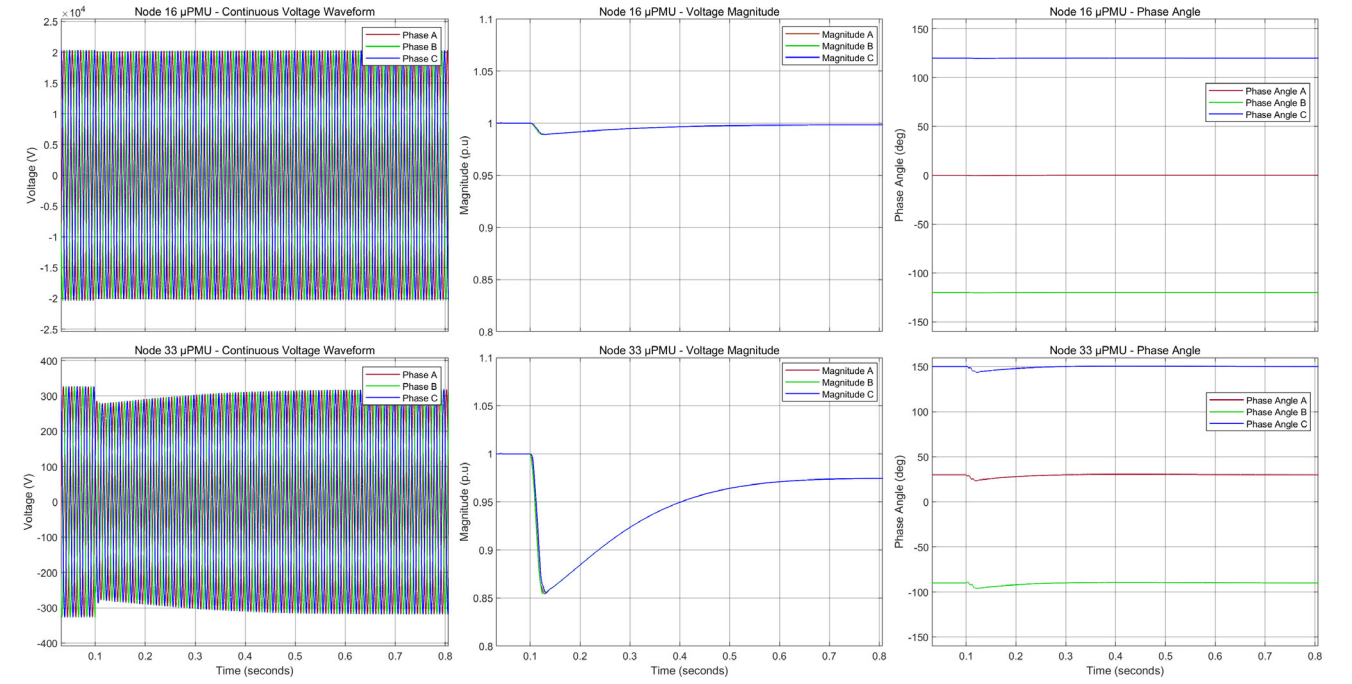

FIGURE 11. Application Case Study 2 – Induction Motor Direct On-Line (DOL) Starting - IEEE-34 Node Test Network, Node 16 μPMU (top) and Node 33 μPMU (bottom); Continuous L-G Voltage Waveform (left), Voltage Magnitude (middle), and Phase Angle (right).

B. APPLICATION CASE STUDY 2 – INDUCTION MOTOR STARTING

A standardized 400V 160 kW squirrel cage induction motor is connected alongside the same load per the previous case study. This situation simulates voltage sag curves due to large induction motor direct on-line (DOL) starting. In Fig. 11, Node 33 μPMU indicates a voltage sag of 0.86 p.u when the motor is connected at 0.1 seconds before settling to steady-state at 0.97 p.u at 0.7 seconds. In contrast, no voltage sag is present at Node 16 μPMU on the HV side, where measurements show a similar voltage drop and recovery curve, but at 0.99 p.u as the disturbance propagates from the LV to the HV side of the transformer. Table 11 shows the 100% OCA results for this scenario. Moreover, 100 additional DOL motor starting scenarios (voltage drops, sags, and normal) were tested with 100% accuracy. This case study highlights

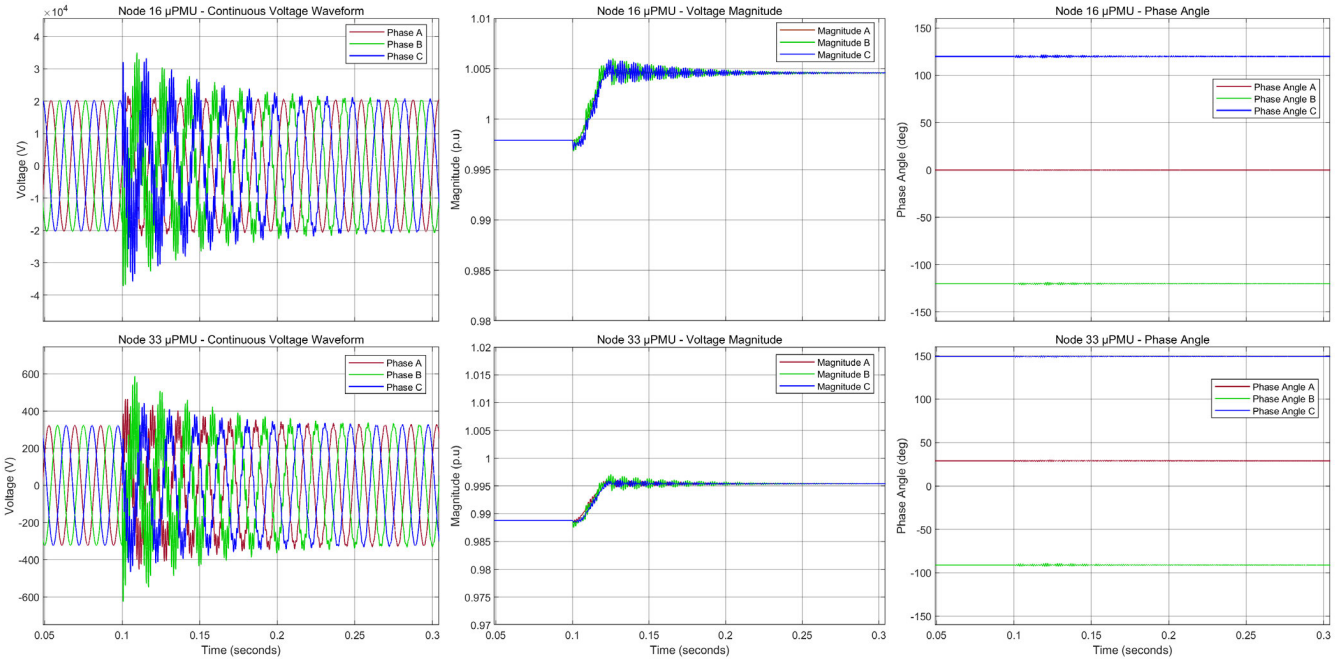

FIGURE 12. Application Case Study 3 – Capacitor Energizing HV Side - IEEE-34 Node Test Network, Node 16 μPMU (top) and Node 33 μPMU (bottom); Continuous L-G Voltage Waveform (left), Voltage Magnitude (middle), and Phase Angle (right).

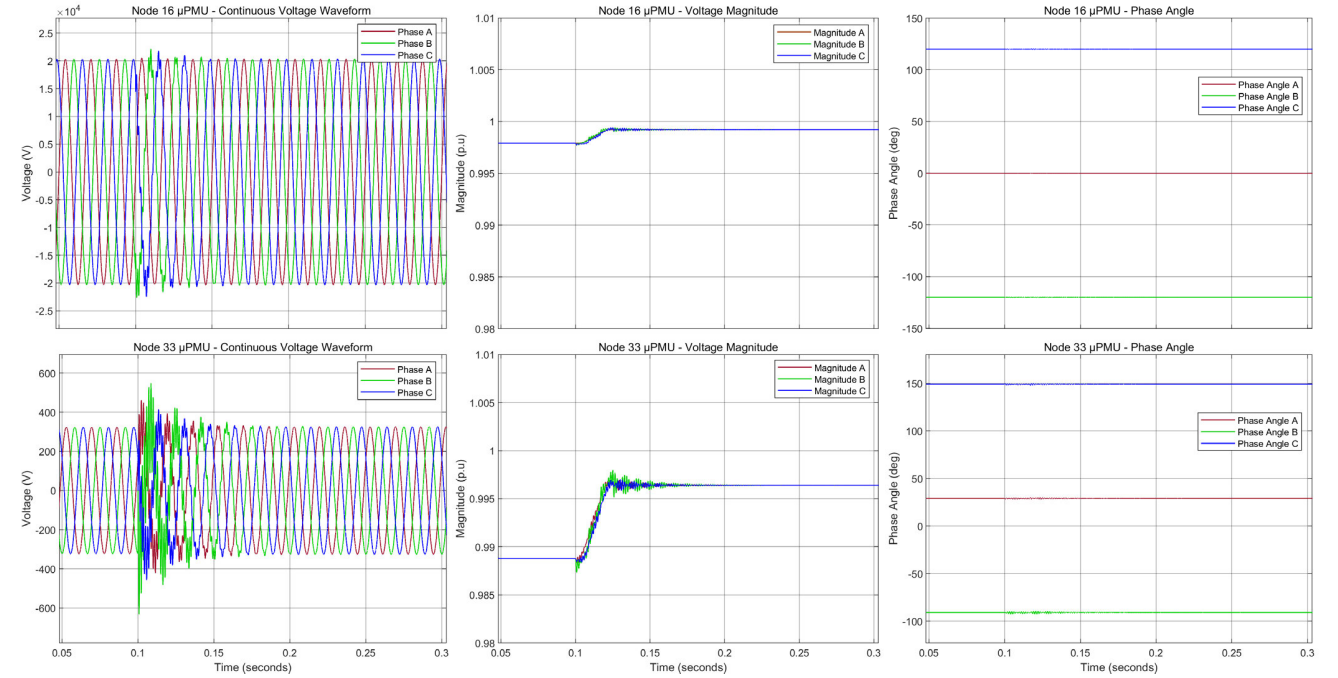

FIGURE 13. Application Case Study 3 – Capacitor Energizing LV Side - IEEE-34 Node Test Network, Node 16 μPMU (top) and Node 33 μPMU (bottom); Continuous L-G Voltage Waveform (left), Voltage Magnitude (middle), and Phase Angle (right).

the importance of μPMU placement closer to critical radial loads, which is also considered in the UZIP String optimal μPMU placement algorithm [51].

C. APPLICATION CASE STUDY 3 – CAPACITOR BANK ENERGIZING

By energizing capacitor banks on the HV and LV sides of the transformer, oscillatory transients can be simulated. The energizing start time is at 0.1s. In Fig. 12, the large HV side capacitor energizing causes a severe oscillatory transient that propagates to the LV side. The oscillations are damped over a duration of 0.3 seconds in this example. In Fig. 13, when the LV side capacitor is energized, the oscillatory behavior can also be clearly seen on both sides of the transformer with varying degrees of severity. The duration of the disturbance is around 0.1 seconds.

Table 12 shows identical results for both the LV and HV side. The voltage magnitude after the capacitor is energized is slightly higher than before and is the expected behavior in this scenario. By varying the load and capacitor bank parameters to alter the oscillatory frequency and damping factors, 100 capacitor energizing simulations (50 HV and 50 LV) were conducted with an OCA of 96%. The UZIP String μPMU placement algorithm [51] also considers the location of capacitor banks, making it possible to check equipment health.

TABLE 13. Application Case Study 4 – Non-linear Loads – IEEE-34 Distribution Network with Optimally Placed μPMUs.

Node	16 µPMU		Node	33 µPMU	
Phase	Predicted	True	Phase	Predicted	True
A	C13 - Notch	✓	A	C13 - Notch	✓
B	C13 - Notch	✓	B	C13 - Notch	✓
C	C13 - Notch	✓	C	C13 - Notch	✓
OCA	100%		OCA	100%	

D. APPLICATION CASE STUDY 4 – NON-LINEAR LOADS

A three-phase six-pulse bridge rectifier is now connected at Node 34 with a large inductive load. There is a sizeable periodic notching closer to the load, as shown by Node 33 μPMU in Fig. 14. However, notching is also present on the HV side at Node 16 in this scenario, as shown in Table 13.

The notching waveform signatures, such as location, width, and depth, can be altered by changing the firing angle (30 degrees in this scenario) and the type of load. For instance, a more significant load will cause greater notching depth, and at certain firing angles, notching may not be present at all. Moreover, in other lighter loading conditions, while notching may be present on the LV side, it may not propagate to the HV side and be insignificant. One hundred different notching scenarios, including normal conditions, were also tested by varying parameters within the appropriate limits with an OCA of 100%.

E. APPLICATION CASE STUDY 5 – ELECTRIC ARC FURNACE

An electric arc furnace MATLAB model developed in [107] is connected at Node 34 in addition to the resistive load used in previous case studies. Fig. 15 shows severe flicker, which is clearly visible in the fluctuation of voltage magnitude from the Node 33 μPMU measurements. As the flicker propagates upstream through the transformer, the severity of the flicker is minimized by the time it reaches Node 16 HV side but is still present as per Table 14. The large instantaneous flicker (Pfs) value was between 321 to 377, similar to the real field flicker PQD data shown in Fig. 6.

For 100 different scenarios, the OCA was 94%. Misclassification occurred with extreme cases where the THD is greater than 20% over the 10-cycle window on the LV side, causing it to be misclassified as harmonics instead of flicker. Moreover, borderline flicker cases on HV side were sometimes classified as normal conditions. This misclassification behavior was previously discussed in Sections IV and V.

TABLE 14. Application Case Study 5 – Electric Arc Furnace – IEEE-34 Distribution Network with Optimally Placed μPMUs.

Node	16 µPMU		Node	33 µPMU	
Phase	Predicted	True	Phase	Predicted	True
A	C10 - Flicker	✓	A	C10 - Flicker	✓
B	C10 - Flicker	✓	B	C10 - Flicker	✓
C	C10 - Flicker	✓	C	C10 - Flicker	✓
OCA	100%		OCA	100%	

VII. COMPARATIVE ANALYSIS, LIMITATIONS, PRACTICAL CONSTRAINTS, ADDITIONAL BENEFITS, AND FUTURE RESEARCH DIRECTION

A. COMPARISON TO PREVIOUS LITERATURE

As shown in Table 15, previous literature [3], [7], [9], [10], [12], [14], [17], [22], [23], [27], [28] has failed to incorporate a large subset of high-quality real PQD field data in their classification methods. Consequently, their proposed methods and ability to detect real-world PQDs are limited and unknown.

Compared to previous studies, this research has evaluated the largest amount of the most commonly occurring standard and complex PQDs. In [30], standard plus 11 complex PQDs were considered; however, there is ambiguity in the composition of the complex synthetic PQDs evaluated. Similarly, in [28] the type of transient was not clearly defined.

The classification of single and double PQDs C01-C17 is 98.65%, whereas the classification of complex triple and quadruple PQDs C18-C29 is 79.54%. As more complex PQDs classes are added, the overall OCA will drop. This is the most common problem with traditional ML techniques. While the OCA is lower for the proposed method at 90.74%, other key aspects are missing from all previous studies, which were limited to simulation or experimental setups, or a small subset of legacy PQD field data, and did not address all the 29 PQDs presented in this paper.

As shown in Table 15, under noisy conditions with SNR of 30, the proposed DWT-CMSVM method with a computationally efficient eight-level denoising algorithm performed well, falling 2.40% compared to the clean noise-free signal tested.

Additionally, the effect of MC, and the high-risk nature of incorrect classification for critical applications is introduced in this study to better understand the behaviour of PQD classifiers so they can be tuned for favourable MC. This key aspect is missing from all previous PQD classifier methods.

B. LIMITATIONS

In ADNs, there is a non-linear relationship between the PQD class type and the number of times each class occurs. For example, in the field recordings, sags, swells, and interruptions account for approximately 80% of the total PQDs.

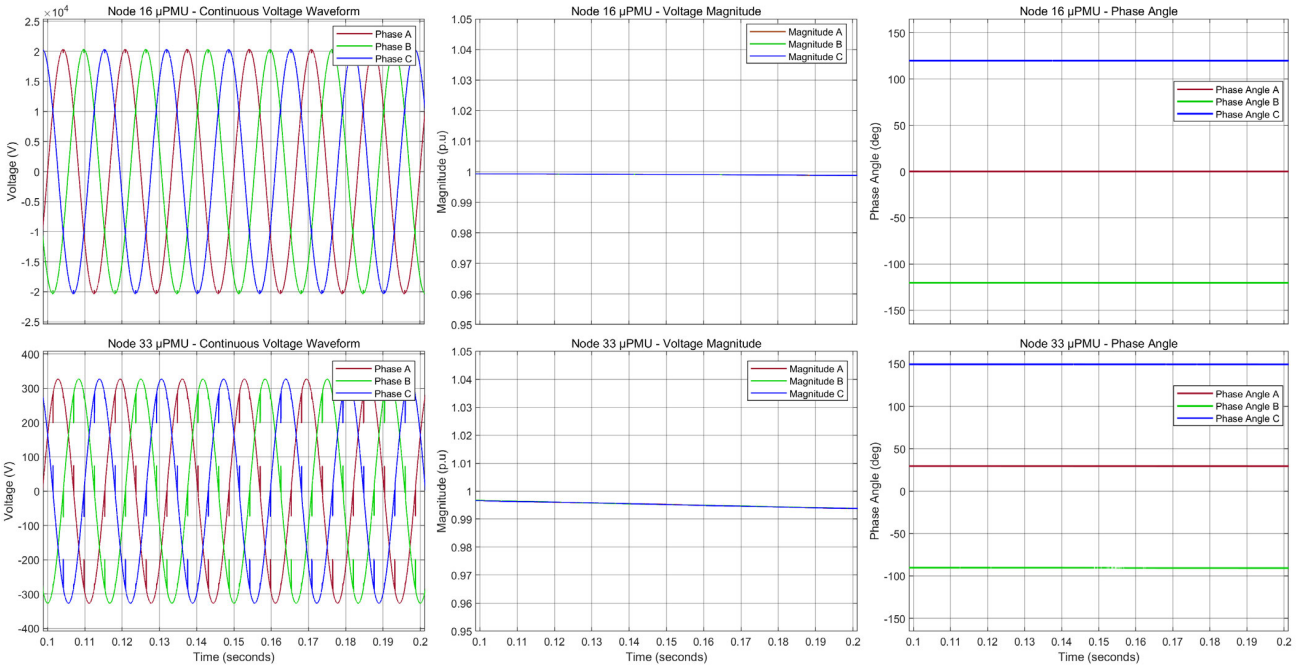

FIGURE 14. Application Case Study 4 – Non-linear Load - Notching - IEEE-34 Node Test Network, Node 16 μPMU (top) and Node 33 μPMU (bottom); Continuous Voltage Waveform (left), Voltage Magnitude (middle), and Phase Angle (right).

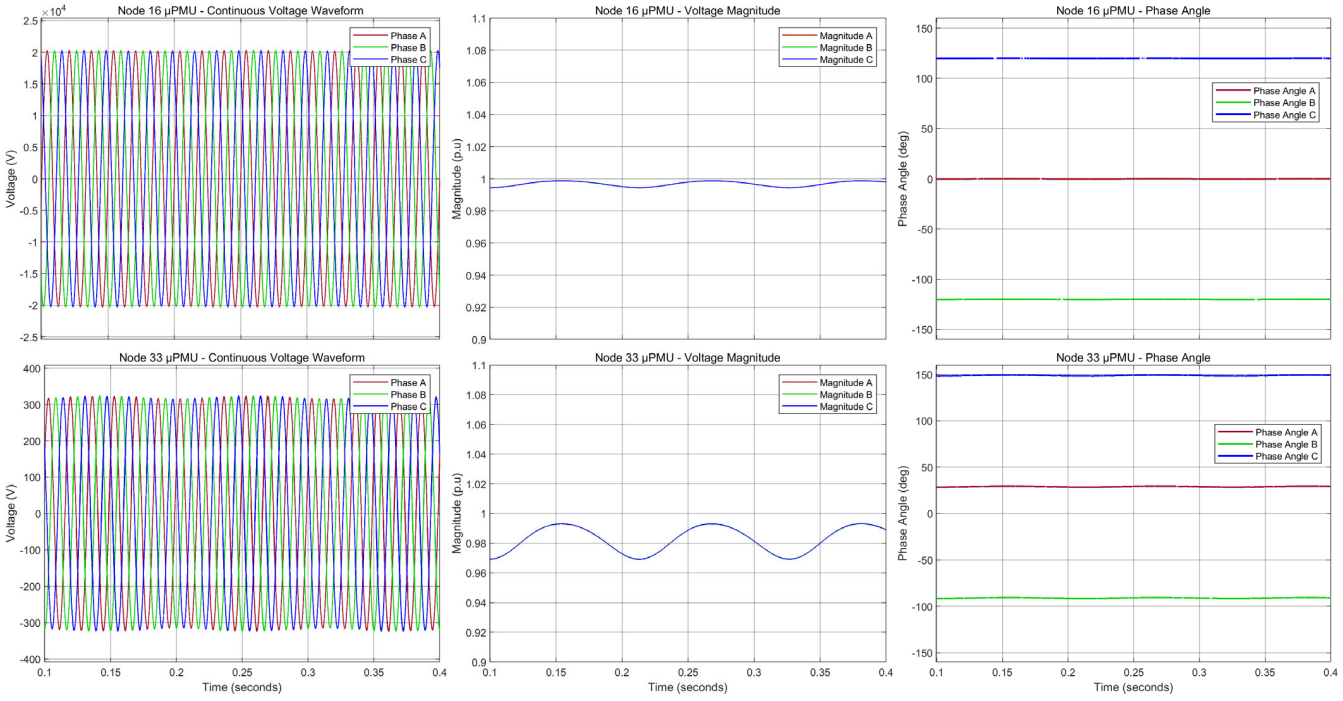

FIGURE 15. Application Case Study 5 – Electric Arc Furnace - Flicker - IEEE-34 Node Test Network, Node 16 μPMU (top) and Node 33 μPMU (bottom); Continuous Voltage Waveform (left), Voltage Magnitude (middle), and Phase Angle (right).

While a few instances of complex PQDs occurred in the field recordings, such as harmonics with flicker with sag, the dataset for complex classes was too small to include in this research or any DL method. Therefore, each PQD class dataset was restricted to a fixed number to understand MC and classifier behavior better. The capture of greater complex field PQDs (tens of thousands) is required to establish a robust classifier.

C. PRACTICAL CONSTRAINTS

Previous studies have added different levels of noise while others have tested their methods under different SNR ratios;

TABLE 15. Comparative Analysis of PQD Classification Methods.

	Previous Literature																						Proposed	
	ST-FFNN		DWT-SVM		ST-DT		ST-PNN		ST-Dyn-DT		ADALINE-FFNN		DWT-SVM		VMD-DT		TQWT-MSVM		DWT-RF		OST-KSVM*		DWT-CMSVM	
Year	2003		2006		2007		2008		2013		2014		2016		2018		2018		2020		2020		2023	
Ref	[7]		[9]		[10]		[12]		[3]		[14]		[17]		[22]		[23]		[27]		[28]			
Real PQD	No		No		No		No		No		No		No		No		No		No		No		Yes	
No. of PQDs	9		7		8		10		11		11		9		13		12		21		16		29	
Noise	NF	N30	NF	N50	N40	N20	NF	N40	NF	N30	NF	N20	NF	N30	NF	N45	NF	N20	NF	N50	NF	N20*	**NF**	**N30**
C01	-	-	100.00	NR	-	-	100.00	94.00	96.00	100.00	100.00	90.00	-	-	-	100.00	-	-	-	NR	100.00	99.83	**100.00**	**97.30**
C02	100.00	100.00	85.50	NR	100.00	97.50	95.00	98.00	95.00	100.00	100.00	98.00	NR	89.00	100.00	100.00	100.00	98.00	-	NR	99.00	95.67	**100.00**	**94.50**
C03	100.00	100.00	100.00	NR	99.50	94.00	91.00	92.00	97.00	100.00	100.00	99.00	NR	89.00	100.00	100.00	100.00	100.00	-	NR	100.00	100.00	**100.00**	**95.10**
C04	100.00	100.00	82.00	NR	99.00	82.00	99.00	99.00	85.00	98.00	100.00	100.00	-	-	100.00	99.35	100.00	100.00	-	NR	99.17	100.00	**100.00**	**99.30**
C05	93.33	100.00	-	-	100.00	96.00	100.00	86.00	94.00	99.00	97.00	90.00	-	-	-	99.00	97.00	94.00	-	NR	100.00	97.83	**100.00**	**99.60**
C06	100.00	53.33	-	-	-	-	-	-	97.00	100.00	98.00	86.00	NR	98.00	100.00	99.16	100.00	94.00	-	NR	100.00	99.17	**98.00**	**97.50**
C07	86.67	86.67	100.00	NR	100.00	98.00	96.00	95.00	97.00	100.00	98.00	90.00	NR	97.00	100.00	100.00	100.00	100.00	-	NR	100.00	100.00	**100.00**	**95.80**
C08	80.00	93.33	96.500	NR	100.00	98.00	98.00	98.00	95.00	99.00	98.00	89.00	NR	97.00	99.00	97.40	98.00	90.00	-	NR	100.00	98.25	**99.10**	**94.30**
C09	80.00	100.00	100.00	NR	99.50	97.00	98.00	84.00	97.00	99.00	97.00	88.00	NR	98.00	99.50	98.62	100.00	100.00	-	NR	99.33	100.00	**99.30**	**94.10**
C10	-	-	-	-	-	-	98.00	82.00	91.00	98.00	94.00	87.00	NR	100.00	99.60	100.00	100.00	100.00	-	NR	100.00	100.00	**99.50**	**91.50**
C11	-	-	-	-	-	-	-	-	-	-	-	-	-	-	-	-	-	-	-	NR	-	-	**98.20**	**96.20**
C12	-	-	-	-	-	-	-	-	-	-	-	-	-	-	-	-	-	-	-	NR	-	-	**98.00**	**89.70**
C13	100.00	100.00	-	-	100.00	95.00	99.00	99.00	94.00	99.00	97.00	85.00	-	-	-	99.00	100.00	100.00	-	NR	100.00	100.00	**100.00**	**100.00**
C14	-	-	-	-	-	-	-	-	-	-	-	-	NR	94.00	-	100.00	92.00	88.00	-	NR	99.00	98.00	**96.30**	**93.30**
C15	-	-	-	-	-	-	-	-	-	-	-	-	NR	94.00	-	100.00	96.00	86.00	-	NR	99.33	98.67	**96.90**	**94.80**
C16	-	-	-	-	-	-	-	-	-	-	-	-	-	-	-	-	-	-	-	-	-	-	**96.10**	**94.60**
C17	-	-	-	-	-	-	-	-	-	-	-	-	-	-	-	-	-	-	-	-	-	-	**95.60**	**94.20**
C18	-	-	-	-	-	-	-	-	-	-	-	-	-	-	-	-	-	-	-	79.30	99.67	98.33	**81.00**	**79.10**
C19	-	-	-	-	-	-	-	-	-	-	-	-	-	-	-	-	-	-	-	81.20	-	-	**83.20**	**78.20**
C20	-	-	-	-	-	-	-	-	-	-	-	-	-	-	-	-	-	-	-	-	-	-	**82.40**	**78.10**
C21	-	-	-	-	-	-	-	-	-	-	-	-	-	-	-	-	-	-	-	-	-	-	**78.30**	**78.70**
C22	-	-	-	-	-	-	-	-	-	-	-	-	-	-	-	-	-	-	-	-	-	-	**83.10**	**80.30**
C23	-	-	-	-	-	-	-	-	-	-	-	-	-	-	-	-	-	-	-	-	-	-	**79.60**	**77.20**
C24	-	-	-	-	-	-	-	-	-	-	-	-	-	-	-	-	-	-	-	67.80	99.67	96.83	**78.80**	**79.80**
C25	-	-	-	-	-	-	-	-	-	-	-	-	-	-	-	-	-	-	-	72.10	99.00	99.00	**80.30**	**79.40**
C26	-	-	-	-	-	-	-	-	-	-	-	-	-	-	-	-	-	-	-	66.20	-	-	**78.90**	**76.70**
C27	-	-	-	-	-	-	-	-	-	-	-	-	-	-	-	-	-	-	-	72.00	-	-	**76.30**	**77.70**
C28	-	-	-	-	-	-	-	-	-	-	-	-	-	-	-	-	-	-	-	-	-	-	**75.50**	**78.10**
C29	-	-	-	-	-	-	-	-	-	-	-	-	-	-	-	-	-	-	-	-	-	-	**77.10**	**76.80**
OCA	93.33	92.59	94.86	94.00	99.75	94.69	97.40	92.70	93.46	99.27	98.09	91.09	NR	95.11	99.76	99.43	98.58	95.83	-	86.78	99.64	98.85	**90.74**	**88.34**

Notes: NR: Not Reported or Overall Classification Accuracy Presented Only; - PQD Case Not Presented; Noise: NF = Noise Free, NXX = SNR, *Type of transient not defined clearly (still reported in Table) & it is unclear whether authors presented SNR or Added Noise in dB, Real-PQD: High quality and large stream of real-life PQD cases used; No. of PQDs: Number of PQDs evaluated from standard and complex PQDs presented; OCA: Overall classification accuracy average in percentage

these quantities are not comparable and are not indicative of real-world PQ measurements.

For example, the field data from the output of the Elspec DFRs, PQAs, and μPMUs used in this paper contained high SNR and less noise. This is due to the filtering embedded in the instrument itself, which also needs to be considered. Therefore, as previous studies have done, it is not reasonable to test PQ classifiers using arbitrary SNRs.

Moreover, PQ monitoring in ADNs requires tighter tolerance to capture useful information. Thus, simulating large amounts of noise is redundant. For instance, for PQ monitoring, a Class M μPMU will be used over Class P due to greater filtering. Other practical constraints that influence PQ measurement accuracy and noise, are the type of potential transformer (PT) or current transformer (CT) class used, burden, and impedance matching.

D. ADDITIONAL INSIGHTS USING OPTIMALLY PLACED MICRO-PMUs

The method presented in this paper also have added PQ insights when μPMUs are optimally placed in the distribution network. In [51], an advanced μPMU placement technique for ADNs considering UDNA elements was established. By placing optimally placed μPMUs and gathering voltage sag characteristics using the PQ insights methods presented in this paper, it is also possible to have additional benefits such as accurate fault detection and localization using ML techniques. This is an area of future research.

E. FUTURE RESEARCH DIRECTION: DEEP LEARNING WITH REAL FIELD DATA

DL methods are the future of PQD classification. However, there are major hurdles, such as the complexity of network models, overfitting, and the lack of high-quality field PQDs to make them suitable for deployment. Overfitting occurs when the model has been trained too well on a specific PQD training dataset, to the point where it has memorized the PQD training data but has not generalized well to new PQD data.

Thus, it will perform well on the training data but struggle with new field PQDs. Moreover, [31] has brought to light the inherent difficulty for PQ specialists to assess the trustworthiness of a particular ML method over another. Therefore, the large-scale deployment of any PQD classification method has been limited.

In this aspect, traditional techniques, such as the proposed method with better MC, can be used to collect complex PQDs making it easier to manually label PQ events for DL methods collected from optimally placed DFRs, PQAs, and μPMUs.

VIII. CONCLUSION

With optimal placement of measurement devices, the use of real-time and historical PQ monitoring tools and an improved PQD classification method can potentially improve the stability and reliability of the smart grid. This research has incorporated high-quality real PQD field data, an improved feature set and a computationally efficient extraction and noise-filtering process. The proposed method showed similar performance to previous literature in OCA of standard PQDs, while improving the MC for complex PQD through cost-sensitive analysis, which was also introduced in this research. This research also demonstrated the importance of training and testing PQD classifiers using real field data to improve the fidelity and trustworthiness of PQD classifiers. Moreover, by conducting five application case studies, it was found that the optimal placement of μPMUs in ADNs is critical to provide additional valuable PQ insights to DSOs. The proposed method can be used to collect standard and complex PQDs from the field to establish a robust DL PQD classification method in the future as more complex components are added to the distribution network.

ACKNOWLEDGMENT

The authors would like to thank Supreme Technology & Energy Solutions Australia Pty Ltd., the distributors for ELSPEC Ltd. products, who provided the power quality field data recorded with ELSPEC G5PMU Phasor Measurement Unit, G5DFR Multi-Functional Digital Fault Recorder, G4430 Blackbox, G4500 Blackbox, and Pure BlackBox (Pure-BB) Power Quality Analyzers with PQSCADA Sapphire Power Management Software Enterprise Edition used in this research.

REFERENCES

[1] R. K. Beniwal, M. K. Saini, A. Nayyar, B. Qureshi, and A. Aggarwal, "A critical analysis of methodologies for detection and classification of power quality events in smart grid," *IEEE Access*, vol. 9, pp. 83507–83534, 2021, doi: 10.1109/ACCESS.2021.3087016.

[2] F. B. Costa, "Boundary wavelet coefficients for real-time detection of transients induced by faults and power-quality disturbances," *IEEE Trans. Power Del.*, vol. 29, no. 6, pp. 2674–2687, Dec. 2014, doi: 10.1109/TPWRD.2014.2321178.

[3] S. He, K. Li, and M. Zhang, "A real-time power quality disturbances classification using hybrid method based on S-transform and dynamics," *IEEE Trans. Instrum. Meas.*, vol. 62, no. 9, pp. 2465–2475, Sep. 2013, doi: 10.1109/TIM.2013.2258761.

[4] P. Castello, C. Muscas, P. A. Pegoraro, D. Sitzia, S. Sulis, G. M. Giannuzzi, M. Pede, C. Maiolini, P. Pau, F. Bassi, and C. Coluzzi, "Enhanced PMU-based wide area measurement system with integrated power quality and fault analysis," in *Proc. Int. Conf. Smart Grid Synchronized Meas. Anal. (SGSMA)*, May 2022, pp. 1–6, doi: 10.1109/SGSMA51733.2022.9806008.

[5] S. Santoso, E. J. Powers, W. M. Grady, and A. C. Parsons, "Power quality disturbance waveform recognition using wavelet-based neural classifier. I. Theoretical foundation," *IEEE Trans. Power Del.*, vol. 15, no. 1, pp. 222–228, Jan. 2000, doi: 10.1109/61.847255.

[6] P. K. Dash, B. K. Panigrahi, D. K. Sahoo, and G. Panda, "Power quality disturbance data compression, detection, and classification using integrated spline wavelet and S-transform," *IEEE Trans. Power Del.*, vol. 18, no. 2, pp. 595–600, Apr. 2003, doi: 10.1109/TPWRD.2002.803824.

[7] I. W. C. Lee and P. K. Dash, "S-transform-based intelligent system for classification of power quality disturbance signals," *IEEE Trans. Ind. Electron.*, vol. 50, no. 4, pp. 800–805, Aug. 2003, doi: 10.1109/TIE.2003.814991.

[8] Z.-L. Gaing, "Wavelet-based neural network for power disturbance recognition and classification," *IEEE Trans. Power Del.*, vol. 19, no. 4, pp. 1560–1568, Oct. 2004, doi: 10.1109/TPWRD.2004.835281.

[9] H. He and J. A. Starzyk, "A self-organizing learning array system for power quality classification based on wavelet transform," *IEEE Trans. Power Del.*, vol. 21, no. 1, pp. 286–295, Jan. 2006, doi: 10.1109/TPWRD.2005.852392.

[10] F. Zhao and R. Yang, "Power-quality disturbance recognition using S-transform," *IEEE Trans. Power Del.*, vol. 22, no. 2, pp. 944–950, Apr. 2007, doi: 10.1109/TPWRD.2006.881575.

[11] W.-M. Lin, C.-H. Wu, C.-H. Lin, and F.-S. Cheng, "Detection and classification of multiple power-quality disturbances with wavelet multiclass SVM," *IEEE Trans. Power Del.*, vol. 23, no. 4, pp. 2575–2582, Oct. 2008, doi: 10.1109/TPWRD.2008.923463.

[12] S. Mishra, C. N. Bhende, and B. K. Panigrahi, "Detection and classification of power quality disturbances using S-transform and probabilistic neural network," *IEEE Trans. Power Del.*, vol. 23, no. 1, pp. 280–287, Jan. 2008, doi: 10.1109/TPWRD.2007.911125.

[13] U. D. Dwivedi and S. N. Singh, "Enhanced detection of power-quality events using intra and interscale dependencies of wavelet coefficients," *IEEE Trans. Power Del.*, vol. 25, no. 1, pp. 358–366, Jan. 2010, doi: 10.1109/TPWRD.2009.2027482.

[14] M. Valtierra-Rodriguez, R. de Jesus Romero-Troncoso, R. A. Osornio-Rios, and A. Garcia-Perez, "Detection and classification of single and combined power quality disturbances using neural networks," *IEEE Trans. Ind. Electron.*, vol. 61, no. 5, pp. 2473–2482, May 2014, doi: 10.1109/TIE.2013.2272276.

[15] M. S. Manikandan, S. R. Samantaray, and I. Kamwa, "Detection and classification of power quality disturbances using sparse signal decomposition on hybrid dictionaries," *IEEE Trans. Instrum. Meas.*, vol. 64, no. 1, pp. 27–38, Jan. 2015, doi: 10.1109/TIM.2014.2330493.

[16] F. A. S. Borges, R. A. S. Fernandes, I. N. Silva, and C. B. S. Silva, "Feature extraction and power quality disturbances classification using smart meters signals," *IEEE Trans. Ind. Informat.*, vol. 12, no. 2, pp. 824–833, Apr. 2016, doi: 10.1109/TII.2015.2486379.

[17] M. D. Borrás, J. C. Bravo, and J. C. Montaño, "Disturbance ratio for optimal multi-event classification in power distribution networks," *IEEE Trans. Ind. Electron.*, vol. 63, no. 5, pp. 3117–3124, May 2016, doi: 10.1109/TIE.2016.2521615.

[18] J. Li, Z. Teng, Q. Tang, and J. Song, "Detection and classification of power quality disturbances using double resolution S-transform and DAG-SVMs," *IEEE Trans. Instrum. Meas.*, vol. 65, no. 10, pp. 2302–2312, Oct. 2016, doi: 10.1109/TIM.2016.2578518.

[19] S. Khokhar, A. A. M. Zin, A. P. Memon, and A. S. Mokhtar, "A new optimal feature selection algorithm for classification of power quality disturbances using discrete wavelet transform and probabilistic neural network," *Measurement*, vol. 95, pp. 246–259, Jan. 2017, doi: 10.1016/j.measurement.2016.10.013.

[20] A. Mejia-Barron, J. P. Amezquita-Sanchez, A. Dominguez-Gonzalez, M. Valtierra-Rodriguez, J. R. Razo-Hernandez, and D. Granados-Lieberman, "A scheme based on PMU data for power quality disturbances monitoring," in *Proc. 43rd Annu. Conf. IEEE Ind. Electron. Soc. (IECON)*, Oct. 2017, pp. 3270–3275, doi: 10.1109/IECON.2017.8216553.

[21] N. Mohan, K. P. Soman, and R. Vinayakumar, "Deep power: Deep learning architectures for power quality disturbances classification," in *Proc. Int. Conf. Technol. Adv. Power Energy (TAP Energy)*, Dec. 2017, pp. 1–6, doi: 10.1109/TAPENERGY.2017.8397249.

[22] P. D. Achlerkar, S. R. Samantaray, and M. S. Manikandan, "Variational mode decomposition and decision tree based detection and classification of power quality disturbances in grid-connected distributed generation system," *IEEE Trans. Smart Grid*, vol. 9, no. 4, pp. 3122–3132, Jul. 2018, doi: 10.1109/TSG.2016.2626469.

[23] K. Thirumala, M. S. Prasad, T. Jain, and A. C. Umarikar, "Tunable-Q wavelet transform and dual multiclass SVM for online automatic detection of power quality disturbances," *IEEE Trans. Smart Grid*, vol. 9, no. 4, pp. 3018–3028, Jul. 2018, doi: 10.1109/TSG.2016.2624313.

[24] K. Cai, W. Cao, L. Aarniovuori, H. Pang, Y. Lin, and G. Li, "Classification of power quality disturbances using Wigner–Ville distribution and deep convolutional neural networks," *IEEE Access*, vol. 7, pp. 119099–119109, 2019, doi: 10.1109/ACCESS.2019.2937193.

[25] L. Lin, D. Wang, S. Zhao, L. Chen, and N. Huang, "Power quality disturbance feature selection and pattern recognition based on image enhancement techniques," *IEEE Access*, vol. 7, pp. 67889–67904, 2019, doi: 10.1109/ACCESS.2019.2917886.

[26] J. Wang, Z. Xu, and Y. Che, "Power quality disturbance classification based on compressed sensing and deep convolution neural networks," *IEEE Access*, vol. 7, pp. 78336–78346, 2019, doi: 10.1109/ACCESS.2019.2922367.

[27] M. Markovska, D. Taskovski, Z. Kokolanski, V. Dimchev, and B. Velkovski, "Real-time implementation of optimized power quality events classifier," *IEEE Trans. Ind. Appl.*, vol. 56, no. 4, pp. 3431–3442, Jul. 2020, doi: 10.1109/TIA.2020.2991950.

[28] Q. Tang, W. Qiu, and Y. Zhou, "Classification of complex power quality disturbances using optimized S-transform and kernel SVM," *IEEE Trans. Ind. Electron.*, vol. 67, no. 11, pp. 9715–9723, Nov. 2020, doi: 10.1109/TIE.2019.2952823.

[29] A. Eisenmann, T. Streubel, and K. Rudion, "An investigation on feature extraction and feature selection for power quality classification with high resolution and RMS data," in *Proc. 9th Renew. Power Gener. Conf.*, Mar. 2021, pp. 377–382, doi: 10.1049/icp.2021.1392.

[30] Y. Liu, T. Jin, M. A. Mohamed, and Q. Wang, "A novel three-step classification approach based on time-dependent spectral features for complex power quality disturbances," *IEEE Trans. Instrum. Meas.*, vol. 70, pp. 1–14, 2021, doi: 10.1109/TIM.2021.3050187.

[31] R. Machlev, M. Perl, J. Belikov, K. Y. Levy, and Y. Levron, "Measuring explainability and trustworthiness of power quality disturbances classifiers using XAI—Explainable artificial intelligence," *IEEE Trans. Ind. Informat.*, vol. 18, no. 8, pp. 5127–5137, Aug. 2022, doi: 10.1109/TII.2021.3126111.

[32] Z. Liu, Y. Cui, and W. Li, "A classification method for complex power quality disturbances using EEMD and rank wavelet SVM," *IEEE Trans. Smart Grid*, vol. 6, no. 4, pp. 1678–1685, Jul. 2015, doi: 10.1109/TSG.2015.2397431.

[33] H. Erişti, Ö. Yıldırım, B. Erişti, and Y. Demir, "Optimal feature selection for classification of the power quality events using wavelet transform and least squares support vector machines," *Int. J. Electr. Power Energy Syst.*, vol. 49, pp. 95–103, Jul. 2013, doi: 10.1016/j.ijepes.2012.12.018.

[34] P. G. V. Axelberg, I. Y.-H. Gu, and M. H. J. Bollen, "Support vector machine for classification of voltage disturbances," *IEEE Trans. Power Del.*, vol. 22, no. 3, pp. 1297–1303, Jul. 2007, doi: 10.1109/TPWRD.2007.900065.

[35] P. Castello, C. Muscas, P. A. Pegoraro, S. Sulis, G. M. Giannuzzi, M. Pede, C. Maiolini, P. Pau, F. Bassi, and C. Coluzzi, "Integration of power quality and fault data into a PMU-based wide area monitoring system," in *Proc. IEEE 11th Int. Workshop Appl. Meas. Power Syst. (AMPS)*, Sep. 2021, pp. 1–5, doi: 10.1109/AMPS50177.2021.9586044.

[36] C. Cui, Y. Duan, H. Hu, L. Wang, and Q. Liu, "Detection and classification of multiple power quality disturbances using Stockwell transform and deep learning," *IEEE Trans. Instrum. Meas.*, vol. 71, pp. 1–12, 2022, doi: 10.1109/TIM.2022.3214284.

[37] D. Gu, Y. Gao, Y. Li, Y. Zhu, and C. Wu, "A novel label-guided attention method for multilabel classification of multiple power quality disturbances," *IEEE Trans. Ind. Informat.*, vol. 18, no. 7, pp. 4698–4706, Jul. 2022, doi: 10.1109/TII.2021.3115567.

[38] Z. Li, H. Liu, J. Zhao, T. Bi, and Q. Yang, "A power system disturbance classification method robust to PMU data quality issues," *IEEE Trans. Ind. Informat.*, vol. 18, no. 1, pp. 130–142, Jan. 2022, doi: 10.1109/TII.2021.3072397.

[39] P. Khetarpal, N. Nagpal, M. S. Al-Numay, P. Siano, Y. Arya, and N. Kassarwani, "Power quality disturbances detection and classification based on deep convolution auto-encoder networks," *IEEE Access*, vol. 11, pp. 46026–46038, 2023, doi: 10.1109/ACCESS.2023.3274732.

[40] M. Liu, Y. Chen, Z. Zhang, and S. Deng, "Classification of power quality disturbance using segmented and modified S-transform and DCNN-MSVM hybrid model," *IEEE Access*, vol. 11, pp. 890–899, 2023, doi: 10.1109/ACCESS.2022.3233767.

[41] Y. Liu, D. Yuan, H. Fan, T. Jin, and M. A. Mohamed, "A multi-dimensional feature-driven ensemble model for accurate classification of complex power quality disturbance," *IEEE Trans. Instrum. Meas.*, vol. 72, pp. 1–13, 2023, doi: 10.1109/TIM.2023.3265756.

[42] T. Ravi and K. S. Kumar, "Detection and classification of power quality disturbances using stock well transform and improved grey wolf optimization-based kernel extreme learning machine," *IEEE Access*, vol. 11, pp. 61710–61727, 2023, doi: 10.1109/ACCESS.2023.3286308.

[43] N. M. Rodrigues, F. M. Janeiro, and P. M. Ramos, "Deep learning for power quality event detection and classification based on measured grid data," *IEEE Trans. Instrum. Meas.*, vol. 72, pp. 1–11, 2023, doi: 10.1109/TIM.2023.3293555.

[44] K. Zhu, Z. Teng, W. Qiu, Q. Tang, and W. Yao, "Complex disturbances identification: A novel PQDs decomposition and modeling method," *IEEE Trans. Ind. Electron.*, vol. 70, no. 6, pp. 6356–6365, Jun. 2023, doi: 10.1109/TIE.2022.3194575.

[45] H. Lu, Y. Xu, M. Ye, K. Yan, Z. Gao, and Q. Jin, "Learning misclassification costs for imbalanced classification on gene expression data," *BMC Bioinf.*, vol. 20, no. S25, p. 681, Dec. 2019, doi: 10.1186/s12859-019-3255-x.

[46] I. Parvez, M. Aghili, A. I. Sarwat, S. Rahman, and F. Alam, "Online power quality disturbance detection by support vector machine in smart meter," *J. Mod. Power Syst. Clean Energy*, vol. 7, no. 5, pp. 1328–1339, Sep. 2019, doi: 10.1007/s40565-018-0488-z.

[47] Elspec. (2023). *G5PMU Phasor Measurement Unit (PMU), G5DFR Multi-Functional Digital Fault Recorder*. [Online]. Available: https://www.elspec-ltd.com/metering-protection/g5-phasor-measurement-unit/

[48] H. Chen, L. Zhang, J. Mo, and K. E. Martin, "Synchrophasor-based real-time state estimation and situational awareness system for power system operation," *J. Mod. Power Syst. Clean Energy*, vol. 4, no. 3, pp. 370–382, Jul. 2016, doi: 10.1007/s40565-016-0212-9.

[49] Powerside. *MicroPMU & LV Data Sheet*. Accessed: Jun. 1, 2023. [Online]. Available: https://powerside.com/wp-content/uploads/2023/02/MicroPMU-LV-Synchrophaser-Data-Sheet.pdf

[50] *IEEE/IEC International Standard—Measuring Relays and Protection Equipment—Part 118–1: Synchrophasor for Power Systems—Measurements*, Standard IEC/IEEE 60255-118-1:2018, 2018, pp. 1–78, doi: 10.1109/IEEESTD.2018.8577045.

[51] M. P. Anguswamy, M. Datta, L. Meegahapola, and A. Vahidnia, "Optimal micro-PMU placement in distribution networks considering usable zero-injection phase strings," *IEEE Trans. Smart Grid*, vol. 13, no. 5, pp. 3662–3675, Sep. 2022, doi: 10.1109/TSG.2022.3174917.

[52] M. Zhang, K. Li, and Y. Hu, "A real-time classification method of power quality disturbances," *Electr. Power Syst. Res.*, vol. 81, no. 2, pp. 660–666, Feb. 2011, doi: 10.1016/j.epsr.2010.10.032.

[53] N. C. F. Tse, J. Y. C. Chan, W.-H. Lau, and L. L. Lai, "Hybrid wavelet and Hilbert transform with frequency-shifting decomposition for power quality analysis," *IEEE Trans. Instrum. Meas.*, vol. 61, no. 12, pp. 3225–3233, Dec. 2012, doi: 10.1109/TIM.2012.2211474.

[54] M. Biswal and P. K. Dash, "Detection and characterization of multiple power quality disturbances with a fast S-transform and decision tree based classifier," *Digit. Signal Process.*, vol. 23, no. 4, pp. 1071–1083, Jul. 2013, doi: 10.1016/j.dsp.2013.02.012.

[55] R. Kumar, B. Singh, and D. T. Shahani, "Recognition of single-stage and multiple power quality events using Hilbert–Huang transform and probabilistic neural network," *Electr. Power Compon. Syst.*, vol. 43, no. 6, pp. 607–619, Apr. 2015, doi: 10.1080/15325008.2014.999147.

[56] R. Kumar, B. Singh, D. T. Shahani, A. Chandra, and K. Al-Haddad, "Recognition of power-quality disturbances using S-transform-based ANN classifier and rule-based decision tree," *IEEE Trans. Ind. Appl.*, vol. 51, no. 2, pp. 1249–1258, Mar. 2015, doi: 10.1109/TIA.2014.2356639.

[57] R. Kumar, B. Singh, and D. T. Shahani, "Symmetrical components-based modified technique for power-quality disturbances detection and classification," *IEEE Trans. Ind. Appl.*, vol. 52, no. 4, pp. 3443–3450, Jul. 2016, doi: 10.1109/TIA.2016.2536665.

[58] M. Lopez-Ramirez, L. Ledesma-Carrillo, E. Cabal-Yepez, C. Rodriguez-Donate, H. Miranda-Vidales, and A. Garcia-Perez, "EMD-based feature extraction for power quality disturbance classification using moments," *Energies*, vol. 9, no. 7, p. 565, Jul. 2016, doi: 10.3390/en9070565.

[59] O. P. Mahela and A. G. Shaik, "Recognition of power quality disturbances using S-transform based ruled decision tree and fuzzy C-means clustering classifiers," *Appl. Soft Comput.*, vol. 59, pp. 243–257, Oct. 2017, doi: 10.1016/j.asoc.2017.05.061.

[60] U. Singh and S. N. Singh, "Application of fractional Fourier transform for classification of power quality disturbances," *IET Sci., Meas. Technol.*, vol. 11, no. 1, pp. 67–76, Jan. 2017, doi: 10.1049/iet-smt.2016.0194.

[61] U. Singh and S. N. Singh, "Detection and classification of power quality disturbances based on time–frequency-scale transform," *IET Sci., Meas. Technol.*, vol. 11, no. 6, pp. 802–810, Sep. 2017, doi: 10.1049/iet-smt.2016.0395.

[62] B. Eristi, O. Yildirim, H. Eristi, and Y. Demir, "A new embedded power quality event classification system based on the wavelet transform," *Int. Trans. Electr. Energy Syst.*, vol. 28, no. 9, Sep. 2018, Art. no. e2597, doi: 10.1002/etep.2597.

[63] E. G. Ribeiro, T. M. Mendes, G. L. Dias, E. R. S. Faria, F. M. Viana, B. H. G. Barbosa, and D. D. Ferreira, "Real-time system for automatic detection and classification of single and multiple power quality disturbances," *Measurement*, vol. 128, pp. 276–283, Nov. 2018, doi: 10.1016/j.measurement.2018.06.059.

[64] K. Cai, T. Hu, W. Cao, and G. Li, "Classifying power quality disturbances based on phase space reconstruction and a convolutional neural network," *Appl. Sci.*, vol. 9, no. 18, p. 3681, Sep. 2019, doi: 10.3390/app9183681.

[65] M. Sahani and P. K. Dash, "FPGA-based online power quality disturbances monitoring using reduced-sample HHT and class-specific weighted RVFLN," *IEEE Trans. Ind. Informat.*, vol. 15, no. 8, pp. 4614–4623, Aug. 2019, doi: 10.1109/TII.2019.2892873.

[66] U. Singh and S. N. Singh, "A new optimal feature selection scheme for classification of power quality disturbances based on ant colony framework," *Appl. Soft Comput.*, vol. 74, pp. 216–225, Jan. 2019, doi: 10.1016/j.asoc.2018.10.017.

[67] K. Thirumala, S. Pal, T. Jain, and A. C. Umarikar, "A classification method for multiple power quality disturbances using EWT based adaptive filtering and multiclass SVM," *Neurocomputing*, vol. 334, pp. 265–274, Mar. 2019, doi: 10.1016/j.neucom.2019.01.038.

[68] O. P. Mahela, B. Khan, H. H. Alhelou, and P. Siano, "Power quality assessment and event detection in distribution network with wind energy penetration using stockwell transform and fuzzy clustering," *IEEE Trans. Ind. Informat.*, vol. 16, no. 11, pp. 6922–6932, Nov. 2020, doi: 10.1109/TII.2020.2971709.

[69] O. Cortes-Robles, E. Barocio, A. Obushevs, P. Korba, and F. R. S. Sevilla, "Fast-training feedforward neural network for multi-scale power quality monitoring in power systems with distributed generation sources," *Measurement*, vol. 170, Jan. 2021, Art. no. 108690, doi: 10.1016/j.measurement.2020.108690.

[70] W. L. R. Junior, F. A. S. Borges, R. D. A. L. Rabelo, J. J. P. C. Rodrigues, R. A. S. Fernandes, and I. N. Silva, "A methodology for detection and classification of power quality disturbances using a real-time operating system in the context of home energy management systems," *Int. J. Energy Res.*, vol. 45, no. 1, pp. 203–219, Jan. 2021, doi: 10.1002/er.5183.

[71] M. Sahani and P. K. Dash, "FPGA-based deep convolutional neural network of process adaptive VMD data with online sequential RVFLN for power quality events recognition," *IEEE Trans. Power Electron.*, vol. 36, no. 4, pp. 4006–4015, Apr. 2021, doi: 10.1109/TPEL.2020.3023770.

[72] P. Janik and T. Lobos, "Automated classification of power-quality disturbances using SVM and RBF networks," *IEEE Trans. Power Del.*, vol. 21, no. 3, pp. 1663–1669, Jul. 2006, doi: 10.1109/TPWRD.2006.874114.

[73] H. Erişti, Ö. Yıldırım, B. Erişti, and Y. Demir, "Automatic recognition system of underlying causes of power quality disturbances based on S-transform and extreme learning machine," *Int. J. Electr. Power Energy Syst.*, vol. 61, pp. 553–562, Oct. 2014, doi: 10.1016/j.ijepes.2014.04.010.

[74] A. A. Abdelsalam, A. A. Eldesouky, and A. A. Sallam, "Characterization of power quality disturbances using hybrid technique of linear Kalman filter and fuzzy-expert system," *Electr. Power Syst. Res.*, vol. 83, no. 1, pp. 41–50, Feb. 2012, doi: 10.1016/j.epsr.2011.09.018.

[75] B. Biswal, H. S. Behera, R. Bisoi, and P. K. Dash, "Classification of power quality data using decision tree and chemotactic differential evolution based fuzzy clustering," *Swarm Evol. Comput.*, vol. 4, pp. 12–24, Jun. 2012, doi: 10.1016/j.swevo.2011.12.003.

[76] H. Liu, F. Hussain, Y. Shen, S. Arif, A. Nazir, and M. Abubakar, "Complex power quality disturbances classification via curvelet transform and deep learning," *Electr. Power Syst. Res.*, vol. 163, pp. 1–9, Oct. 2018, doi: 10.1016/j.epsr.2018.05.018.

[77] M. K. Saini and R. K. Beniwal, "Detection and classification of power quality disturbances in wind-grid integrated system using fast time-time transform and small residual-extreme learning machine," *Int. Trans. Electr. Energy Syst.*, vol. 28, no. 4, Apr. 2018, Art. no. e2519, doi: 10.1002/etep.2519.

[78] J. G. M. S. Decanini, M. S. Tonelli-Neto, F. C. V. Malange, and C. R. Minussi, "Detection and classification of voltage disturbances using a fuzzy-ARTMAP-wavelet network," *Electr. Power Syst. Res.*, vol. 81, no. 12, pp. 2057–2065, Dec. 2011, doi: 10.1016/j.epsr.2011.07.018.

[79] M. B. I. Reaz, F. Choong, M. S. Sulaiman, F. Mohd-Yasin, and M. Kamada, "Expert system for power quality disturbance classifier," *IEEE Trans. Power Del.*, vol. 22, no. 3, pp. 1979–1988, Jul. 2007, doi: 10.1109/TPWRD.2007.899774.

[80] S. Jamali, A. R. Farsa, and N. Ghaffarzadeh, "Identification of optimal features for fast and accurate classification of power quality disturbances," *Measurement*, vol. 116, pp. 565–574, Feb. 2018, doi: 10.1016/j.measurement.2017.10.034.

[81] S. A. Deokar and L. M. Waghmare, "Integrated DWT–FFT approach for detection and classification of power quality disturbances," *Int. J. Electr. Power Energy Syst.*, vol. 61, pp. 594–605, Oct. 2014, doi: 10.1016/j.ijepes.2014.04.015.

[82] H. Erişti and Y. Demir, "A new algorithm for automatic classification of power quality events based on wavelet transform and SVM," *Expert Syst. Appl.*, vol. 37, no. 6, pp. 4094–4102, Jun. 2010, doi: 10.1016/j.eswa.2009.11.015.

[83] B. Biswal, P. K. Dash, and B. K. Panigrahi, "Power quality disturbance classification using fuzzy C-means algorithm and adaptive particle swarm optimization," *IEEE Trans. Ind. Electron.*, vol. 56, no. 1, pp. 212–220, Jan. 2009, doi: 10.1109/TIE.2008.928111.

[84] S. Hasheminejad, S. Esmaeili, and S. Jazebi, "Power quality disturbance classification using S-transform and hidden Markov model," *Electr. Power Compon. Syst.*, vol. 40, no. 10, pp. 1160–1182, Jul. 2012, doi: 10.1080/15325008.2012.682250.

[85] T. K. Abdel-Galil, M. Kamel, A. M. Youssef, E. F. El-Saadany, and M. M. A. Salama, "Power quality disturbance classification using the inductive inference approach," *IEEE Trans. Power Del.*, vol. 19, no. 4, pp. 1812–1818, Oct. 2004, doi: 10.1109/TPWRD.2003.822533.

[86] B. Biswal, M. K. Biswal, P. K. Dash, and S. Mishra, "Power quality event characterization using support vector machine and optimization using advanced immune algorithm," *Neurocomputing*, vol. 103, pp. 75–86, Mar. 2013, doi: 10.1016/j.neucom.2012.08.031.

[87] A. Rodríguez, J. A. Aguado, F. Martín, J. J. López, F. Muñoz, and J. E. Ruiz, "Rule-based classification of power quality disturbances using S-transform," *Electr. Power Syst. Res.*, vol. 86, pp. 113–121, May 2012, doi: 10.1016/j.epsr.2011.12.009.

[88] Z.-Y. Li and W.-L. Wu, "Classification of power quality combined disturbances based on phase space reconstruction and support vector machines," *J. Zhejiang Univ. Sci. A*, vol. 9, no. 2, pp. 173–181, Feb. 2008, doi: 10.1631/jzus.A071261.

[89] A. A. Abdoos, P. K. Mianaei, and M. R. Ghadikolaei, "Combined VMD-SVM based feature selection method for classification of power quality events," *Appl. Soft Comput.*, vol. 38, pp. 637–646, Jan. 2016, doi: 10.1016/j.asoc.2015.10.038.

[90] R. Hooshmand and A. Enshaee, "Detection and classification of single and combined power quality disturbances using fuzzy systems oriented by particle swarm optimization algorithm," *Electr. Power Syst. Res.*, vol. 80, no. 12, pp. 1552–1561, Dec. 2010, doi: 10.1016/j.epsr.2010.07.001.

[91] M. Uyar, S. Yildirim, and M. T. Gencoglu, "An expert system based on S-transform and neural network for automatic classification of power quality disturbances," *Expert Syst. Appl.*, vol. 36, no. 3, pp. 5962–5975, Apr. 2009, doi: 10.1016/j.eswa.2008.07.030.

[92] J. Liu, H. Song, H. Sun, and H. Zhao, "High-precision identification of power quality disturbances under strong noise environment based on FastICA and random forest," *IEEE Trans. Ind. Informat.*, vol. 17, no. 1, pp. 377–387, Jan. 2021, doi: 10.1109/TII.2020.2966223.

[93] B. K. Panigrahi and V. R. Pandi, "Optimal feature selection for classification of power quality disturbances using wavelet packet-based fuzzy k-nearest neighbour algorithm," *IET Gener., Transmiss. Distrib.*, vol. 3, no. 3, pp. 296–306, Mar. 2009.

[94] U. Singh and S. N. Singh, "Optimal feature selection via NSGA-II for power quality disturbances classification," *IEEE Trans. Ind. Informat.*, vol. 14, no. 7, pp. 2994–3002, Jul. 2018, doi: 10.1109/TII.2017.2773475.

[95] N. Huang, D. Xu, X. Liu, and L. Lin, "Power quality disturbances classification based on S-transform and probabilistic neural network," *Neurocomputing*, vol. 98, pp. 12–23, Dec. 2012, doi: 10.1016/j.neucom.2011.06.041.

[96] Y. Luo, K. Li, Y. Li, D. Cai, C. Zhao, and Q. Meng, "Three-layer Bayesian network for classification of complex power quality disturbances," *IEEE Trans. Ind. Informat.*, vol. 14, no. 9, pp. 3997–4006, Sep. 2018, doi: 10.1109/TII.2017.2785321.

[97] S.-H. Cho, G. Jang, and S.-H. Kwon, "Time-frequency analysis of power-quality disturbances via the Gabor–Wigner transform," *IEEE Trans. Power Del.*, vol. 25, no. 1, pp. 494–499, Jan. 2010, doi: 10.1109/TPWRD.2009.2034832.

[98] T. Weihown, M. R. Yusoff, M. F. Yaakub, and A. R. Abdullah, "Voltage variations identification using Gabor transform and rule-based classification method," *Int. J. Electr. Comput. Eng.*, vol. 10, no. 1, pp. 681–689, 2020, doi: 10.11591/ijece.v10i1.pp681-689.

[99] H. Eristi and Y. Demir, "Automatic classification of power quality events and disturbances using wavelet transform and support vector machines," *IET Generat., Transmiss., Distrib.*, vol. 6, no. 10, pp. 968–976, Oct. 2012.

[100] J. E. Caicedo, D. Agudelo-Martínez, E. Rivas-Trujillo, and J. Meyer, "A systematic review of real-time detection and classification of power quality disturbances," *Protection Control Mod. Power Syst.*, vol. 8, no. 1, p. 3, Dec. 2023, doi: 10.1186/s41601-023-00277-y.

[101] R. Igual, C. Medrano, F. J. Arcega, and G. Mantescu, "Integral mathematical model of power quality disturbances," in *Proc. 18th Int. Conf. Harmon. Quality Power (ICHQP)*, May 2018, pp. 1–6, doi: 10.1109/ICHQP.2018.8378902.

[102] Elspec. (2023). *G4400/G4430G4500 3-Phase Class A Power Quality Analyzer*. [Online]. Available: https://www.elspec-ltd.com/metering-protection/power-quality-analyzers/g4400-power-quality-analyzer/

[103] *IEEE Recommended Practice for Monitoring Electric Power Quality*, IEEE Standard 1159-2019 (Revision of IEEE Standard 1159-2009), 2019, pp. 1–98, doi: 10.1109/IEEESTD.2019.8796486.

[104] T. P. Tun and G. Pillai, "Power quality event classification in distribution grids using machine learning," in *Proc. 56th Int. Univ. Power Eng. Conf. (UPEC)*, Aug. 2021, pp. 1–6, doi: 10.1109/UPEC50034.2021.9548222.

[105] *IEEE Recommended Practice for the Analysis of Fluctuating Installations on Power Systems*, IEEE Standard 1453-2015 (Revision of IEEE Standard 1453-2011), 2015, pp. 1–74, doi: 10.1109/IEEESTD.2015.7317469.

[106] C. Allioua, F. Costa, A. Mingotti, L. Peretto, and R. Tinarelli, "Open-source MATLAB-based PMU library for HIL applications compliant with IEC/IEEE 60255-118-1," in *Proc. IEEE 12th Int. Workshop Appl. Meas. for Power Syst. (AMPS)*, Sep. 2022, pp. 1–6, doi: 10.1109/AMPS55790.2022.9978837.

[107] H. G. T. Rodney and K. R. Vigna, "A comprehensive modeling and simulation of power quality disturbances using MATLAB/SIMULINK," in *Power Quality Issues in Distributed Generation*, L. Jaroslaw, Ed. Rijeka, Croatia: IntechOpen, 2015, ch. 3.

MANOJ PRABHAKAR ANGUSWAMY (Member, IEEE) received the bachelor's degree (Hons.) in electrical and electronic engineering and the Bachelor of International Business degree (Hons.) from the Royal Melbourne Institute of Technology (RMIT) University, Melbourne, Australia, in 2019, where he is currently pursuing the Ph.D. degree in electrical and electronic engineering. His research interests include the application of synchrophasor technology in smart grid and active distribution networks, state estimation, and power quality solutions. He is a member of the IEEE Power Engineering Society (PES) and a member of Engineers Australia. He has also served as a Peer-Reviewer for IEEE TRANSACTIONS ON SMART GRID and IEEE TRANSACTIONS ON POWER DELIVERY.

MANOJ DATTA (Senior Member, IEEE) received the D.Eng. degree in the interdisciplinary systems from the University of the Ryukyus, Japan, in 2011. From 2011 to 2012, he was a Japan Society for the Promotion of Science Postdoctoral Research Fellow in Japan. From 2012 to 2013, he was an Assistant Professor with the Department of Human and Information Systems, Gifu University, Japan. Since June 2013, he has been with the School of Electrical and Computer Engineering, Royal Melbourne Institute of Technology (RMIT) University, Melbourne, Australia, where he is currently a Senior Lecturer. He was a recipient of the University of the Ryukyus President's Honorary Award for outstanding Ph.D. thesis. He is a member of the Institute of Electrical Engineers, Japan, and Engineers Australia. He is a chartered professional engineer in Australia. He is an Associate Editor of IEEE ACCESS. His research interests include renewable energy systems and microgrid modeling, the grid integration of DGs, and intelligent ancillary services and communication networks in smart grids.

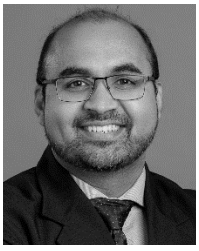

LASANTHA MEEGAHAPOLA (Senior Member, IEEE) received the B.Sc.(Eng.) degree (Hons.) in electrical engineering from the University of Moratuwa, Sri Lanka, in 2006, and the Ph.D. degree from the Queen's University of Belfast, U.K., in 2010.

His doctoral study was based on the investigation of power system stability issues with high wind penetration, and research was conducted in collaboration with EirGrid (Republic of Ireland-TSO). He has over 15 years research experience in power system dynamics and stability with renewable power generation, and he has published over 150 journals and conference papers. He has also conducted research studies on microgrid dynamics and stability, synchrophasor-based stability assessment, and coordinated reactive power dispatch during steady-state and dynamic/transient conditions. He was a Visiting Researcher with the Electricity Research Centre, University College Dublin, Ireland (2009–2010). From 2011 to 2014, he was a Lecturer with the University of Wollongong (UOW) and continued as an Honorary Senior Fellow. He is currently an Associate Professor with the Royal Melbourne Institute of Technology (RMIT) University. He is a member of the IEEE Power Engineering Society (PES) and the IEEE Industry Applications Society. He is also an active member of the IEEE PES Power System Dynamic Performance (PSDP) Committee task forces on microgrid stability analysis and microgrid dynamic modeling and working group on voltage stability. He made key contributions toward identifying and classifying stability issues in microgrids. He is also serving as an Associate Editor for IEEE TRANSACTIONS ON POWER SYSTEMS, IEEE POWER ENGINEERING LETTERS, IEEE TRANSACTIONS ON INDUSTRY APPLICATIONS, and *IET Renewable Power Generation* journals.

ARASH VAHIDNIA (Senior Member, IEEE) received the Ph.D. degree in power engineering from the Queensland University of Technology (QUT). He is currently a Senior Lecturer with the School of Engineering, Royal Melbourne Institute of Technology (RMIT) University. He was a Research Fellow with the Power Engineering Group, QUT, before joining RMIT. He also has several years of industry experience working at power consultancy and utility firms. His research interests include power system stability, reliability, microgrids, renewable energies, and system planning and control.